Relativistic light-matter interaction: Describing the multi-photon ionization process utilizing time dilation

Esther A. B. Johnsen

Master Thesis in Physics

Department of Physics and Technology
University of Bergen

2023

Acknowledgment

First, I would like to thank my supervisor Prof. Morton Førre. Without his enthusiasm, support, and infinite patience through the writing process, this thesis would not have been possible. I want to thank everyone who helped me through the writing process. Especially Adriane Louis Rødfejll and Ingrid Askeland Johnsen, who helped me immensely.

I would also thank all the friends I have made through my studies, who have supported me, let me be myself, and let me info dump on them about my thesis. I would especially like to thank the friends I made in my Nanotechnology bachelor's, our study sessions were always hilarious. Also, I would like to thank Ida-Marie Fauske Johansson who became my first friend in my master's studies and supported me through everything.

I want to thank all the teachers and professors that did not give up and believed in me. I would especially like to thank Jan Inge Vedøy, my science teacher in middle school. Who introduced me to relativity which sparked my interest in physics. Thank you for tolerating me and answering all my questions. I would also like to thank Ellen Salemonsen and Britt Utbjoe Anderssland. You saw me back then, and if it were not for you, I would never have come as far as I've come. Thank you for not giving up on me.

Finally, I want to thank my family and friends, who have supported me immensely through my studies.

Esther A. B. Johnsen
Bergen, January 12th

Abstract

The relativistic multi-photon ionization process is not yet fully understood [1, 2]. As a super-intense X-ray laser pulse ionizes an atom, the electron may achieve relativistic speeds. Hence, as the electron absorbs a multiple number of photons in succession, the system is affected by relativity. This results in the kinetic energy of the electron being increased in comparison to the non-relativistic equivalent, i.e., a relativistic blue shift. By reducing the system to 1D, we studied and singled out what is causing this relativistic blue shift. Finally, we have constructed a model that describes the relativistic mechanisms involved in the multi-photon ionization process by utilizing time dilation.

Contents

Chapter 1

Introduction

In the early 20th century, there were some huge advancements in the scientific community, which revolutionized the way we see, study, and understand the world and universe. In the year 1900, M. Planck solved the problem with the description of black body radiation when he published his paper on the energy distribution law, now known as the Planck distribution. Here he was the first to discuss the quantization of energy by introducing Planck's constant [3, 4]. This became the foundation for what is now known as quantum mechanics. Through the further works of Schrödinger [5], Heisenberg [6], Dirac [7], Bohr [8], Einstein [9], and others, quantum mechanics was developed. Quantum mechanics allows us to study and describe atomic and molecular systems accurately and lays the foundation for quantum chemistry [4].

The quantization of energy was not the only groundbreaking discovery published in the 20th century. In the years 1905-1906, Einstein published four pioneering articles; one related to Planck's description of the quantization of energy, the photoelectric effect [9], one explaining Brownian motion [10], and two introducing the theory of special relativity [11, 12]. The theory of special relativity explains how time, length, and mass are experienced by a moving object and related to its velocity [12] and that the speed of light is always constant and independent of the movement of the source [11]. In 1928 Dirac combined quantum mechanics and special relativity and developed the relativistic Dirac equation [7]. The Dirac equation is central in what's known as relativistic quantum mechanics, and predicts the existence of antimatter as well as the spin of particles.

There were also some significant technological advancements in the middle of the 20th century, opening up new opportunities for studying the dynamics of quantum systems experimentally. One of them was the invention of the laser in 1960 [13]. The first concepts of the laser were actually proposed by Einstein in 1916, where he proposed that photons could stimulate the emission of identical photons from atoms with electrons in an excited state [14]. In 1954 Townes and his student Gordon first demonstrated stimulated emission at the microwave frequency. This was done in a resonance cavity, which amplified the output, also known as a maser (Microwave Amplification by Stimulated Emission of Radiation) [13]. For the next six years, the development of the maser flourished, and some physicists got the idea of extending the principle of the maser to higher frequencies. In 1960, Maiman achieved this and developed the very first ruby laser, which emitted bright red light [13]. Since then, the evolution of the laser-technology has improved immensely, opening up novel opportunities for studying and manipulating quantum systems at a detailed level. The principles of the laser have been extended to even higher frequencies and entered the X-ray range. In later years, after leaps of scientific development, we have achieved incredible laser

intensities [15].

All these discoveries allow us to study and understand systems and phenomena we could not before, like the particle-wave duality of light and matter or the resulting light-matter interaction. The super-intense laser allowed us to study, among other processes, the multi-photon ionization process. As the super-intense X-ray laser pulse ionizes an atom, the electron may absorb multiple photons in succession. This could be considered a generalization of the photon-electric effect. As the electron absorbs photons, we need to consider that the electron may eventually achieve relativistic speeds. In this thesis, we will study the relativistic light-matter interaction involved in the multi-photon ionization process. This process is not yet fully understood [1, 2]. The multi-photon ionization is illustrated in fig. 1.1. The figure depicts the corresponding energy distribution after the net absorption of one (leftmost peak) to seven (rightmost peak) photons from the field. The blue line represents the relativistic process, and the black line represents the non-relativistic one. As seen in the figure, the relativistic result is shifted to higher energies, with respect to the corresponding non-relativistic result, i.e., a relativistic blue shift. The shift is denoted as d in the inset. It was recently found that this relativistic blue shift depended on some of the properties of

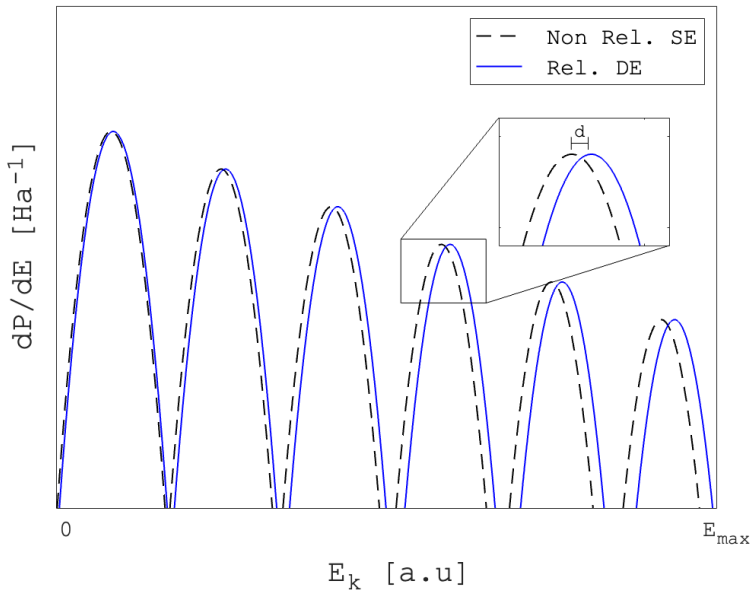

Figure 1.1: A model of the blue shift observed in the energy spectra under the multi-photon ionization process that occurs when a super intense X-ray laser pulse interacts with a hydrogen-like atom. The black line represents energy spectra when solving a non-relativistic equation, and the blue line represents when the relativistic effects are considered.

the laser pulse, such as radiation pressure and intensity, and was described as a temporal relativistic mass shift [1, 2].

In an attempt to understand which mechanisms are involved and which relativistic effect causes the relativistic blue shift, we will study a 1D system. The 1D system can be considered an electron moving inside an extremely thin nanotube [16] within a narrow potential. By reducing the system to 1D, we will first be able to identify if the shift exists in 1D. Then, in a simplified system, we can determine which relativistic effect is causing the relativistic blue shift. By constructing a 1D quantum mechanical model, we can solve the problem in both non-relativistic and relativistic contexts. We will utilize the time-dependent Schrödinger equation and the time-dependent Dirac

equation to simulate the multi-photon ionization process. Furthermore, to be able to single out what's causing the blue shift, we will also construct a relativistic Schrödinger formulation utilizing the Foldy-Wouthuysen transformation [17]. The respective time-dependent problems are then solved numerically by using a particle-in-box basis set expansion. The Crank-Nicholson propagator method is finally used to model the system's time evolution.

This thesis aims to identify and understand the relativistic mechanisms involved in causing this relativistic blue shift in energy. We will then construct a simple model describing the multi-photon ionization process. As the shift seems to be caused by a temporal relativistic effect, we here propose that the shift may be time-dependent and caused by the relativistic effect of time dilation. Utilizing time dilation, we construct a simple model for the multi-photon ionization process and describe how the relativistic blue shift varies with the laser's intensity and angular frequency and how the relativistic blue shift increases for each photon-ionization.

Useful constants

The atomic unit system is often utilized to execute calculations on an atomic scale. In atomic units, the electron's mass, the absolute value of the electron's charge, the reduced Planck constant, and the Bohr radius are set to unity. In table 1.1, we find some of the constants in atomic units and their corresponding value in SI units.

Constant	Physical unit	Symbol	Value (SI)	Value [a.u.]
Electron mass	Mass	m_e	$9.109\,384 \cdot 10^{-31}$ kg	1
Electron charge	Charge	$-e$	$-1.602\,177 \cdot 10^{-19}$ C	-1
Planck constant	Energy · time	h	$6.626\,070 \cdot 10^{-34}$ Js	2π
The reduced Planck constant	Energy · time	$\hbar$	$1.054\,571 \cdot 10^{-34}$ Js	1
Bohr radius	Length	a_0	$5.291\,772 \cdot 10^{-11}$ m	1
Fine structure constant	Unit less	α	$\frac{1}{137.036}$	$\frac{1}{137.036}$
Speed of light	Speed	c	$2.997\,925 \cdot 10^{8}$ m/s	137.036
Energy unit Hartree	Energy	E_h	$4.359\,745 \cdot 10^{-18}$ J	1
Time unit	Time	t	$2.418\,884 \cdot 10^{-17}$ s	1

Table 1.1: Table of useful constants utilized in this thesis and their value in SI units and atomic units (a.u.).

Chapter 2

Theory

2.1 Quantum Mechanics

Not all systems can be described by classical mechanics. For example, classical mechanics is not sufficient to describe a molecular system or systems moving at relativistic speeds. To study these kinds of systems, we must apply quantum mechanics and the theory of relativity, respectively. Here we will go over the basics of quantum mechanics. We will also discuss the postulates defining the Schrödinger picture.

2.1.1 Operators

An operator is a symbol for carrying out a specific action, an operation, on a function or vector. This operation can be almost anything, for example: taking the derivative or multiplying with x [4]. For many of the operators we use, the system is an eigenfunction of the operator. This means that the operation does not change the eigenfunction. The eigenvalue equation is given by

$$\Omega f = \omega f. \tag{2.1}$$

Here Ω is an operator, and ω is the corresponding eigenvalue. We can exploit this eigenfunction relation. If we express g as a linear combination of f functions, $g = \sum_n c_n f_n$, we can calculate Ωg, $\Omega g = \Omega \sum_n c_n f_n$, even though g is not a direct eigenfunction of Ω [4]. Ωg then becomes:

$$\Omega g = \Omega \sum_n c_n f_n = \sum_n c_n \Omega f_n = \sum_n c_n \omega_n f_n \tag{2.2}$$

This becomes quite useful when solving the eigenvalue problems later on. Often operators are directly related to an observable. An observable is any measurable dynamic variable in our system. Examples of this are the momentum operator and the position operator, given by:

$$x \to x\times \tag{2.3}$$

$$p_x \to -i\hbar \frac{\partial}{\partial x} \tag{2.4}$$

Where $\hbar$ is the reduced Planks constant, $\hbar = \frac{h}{2\pi}$ and in atomic units $\hbar = 1$. Applying the p_x operator to a system, which is an eigenfunction to p_x, will produce the system's momentum in the x-direction.

An important feature of operators is that they do not necessarily commute. If two operators, A, and B, do not commute, then $AB \neq BA$. The commutator for A and B, denoted as $[A, B]$, is expressed as follows [4],

$$[A, B] = AB - BA. \tag{2.5}$$

We also have anti-commutator relations given by,

$$\{A, B\} = AB + BA. \tag{2.6}$$

Anti-commutator relations will prove useful later on, for example, when treating the Dirac equation in relativistic quantum mechanics.

Bra-ket notation

To evaluate many types of observables in quantum mechanics, we will need to evaluate an integral over the related operator. These integrals are typical on the form

$$I = \int f_m^* \Omega f_n d\tau, \tag{2.7}$$

where $d\tau$ represents the volume element, so the integral is over all space. For Cartesian coordinates $d\tau = dxdydz$. The bra-ket notation can represent this integral

$$\int f_m^* \Omega f_n d\tau = \langle m|\Omega|n\rangle. \tag{2.8}$$

The $|n\rangle$ is called a ket and denotes the state of f_n, and the $\langle m|$ is called a bra and denotes the complex conjugate state of f_m. Often these represent the initial and final state of the system.

Another useful integral is the overlap integral represented by S:

$$S = \int f_m^* f_n d\tau = \langle m|n\rangle \tag{2.9}$$

We can represent the overlap integral, S, and the integral over the operator, Ω, as matrix elements of the respective matrices $\boldsymbol{S}$ and $\boldsymbol{\Omega}$,

$$\langle m|\Omega|n\rangle = \boldsymbol{\Omega}_{mn} \tag{2.10}$$

$$\langle m|n\rangle = \boldsymbol{S}_{mn} \tag{2.11}$$

Since most of the functions we encounter are normalized and orthogonal, they satisfy the orthogonality condition. The orthogonality condition states that the wave functions of two states of the system, $|m\rangle$ and $|n\rangle$, are orthogonal to each other. Therefore we can express the overlap integral as a delta function,

$$\boldsymbol{S}_{mn} = \langle m|n\rangle = \delta_{mn}. \tag{2.12}$$

Hence, where δ_{mn} represents the delta function, also known as the Kronecker delta. The Kronecker

delta is defined as

$$\delta_{mn} = \begin{cases} 1 & \text{for } m = n \\ 0 & \text{for } m \neq n \end{cases}. \tag{2.13}$$

Another useful feature of the bra-ket notation is, by definition, if $|m\rangle$ and $|n\rangle$ are orthogonal, the complex conjugate of the matrix element $\boldsymbol{S}_{mn}$ is $\boldsymbol{S}^*_{nm}$ [4],

$$\boldsymbol{S}_{mn} = \langle m|n\rangle = \langle n|m\rangle^* = \boldsymbol{S}^*_{nm}, \tag{2.14}$$

this is known as Hermicity.

Hermicity

An operator is hermitian if the following relation is fulfilled:

$$\boldsymbol{\Omega}^*_{mn} = \langle m|\Omega|n\rangle^* = \langle n|\Omega|m\rangle = \boldsymbol{\Omega}_{nm} \tag{2.15}$$

This is only true if the following condition for a hermitian operator is also true [4]:

1. The eigenvalue for a hermitian operator is real.
2. The eigenfunctions corresponding to different eigenvalues for a hermitian operator are orthogonal. To be more concrete, it is always possible to construct an orthogonal set of eigenfunctions for a hermitian operator.

In this project, we will only use hermitian operators.

2.1.2 The postulates of Quantum Mechanics

The postulates of quantum mechanics are statements that are not proven nor provable, but they are the basis for all quantum physics. In this thesis, we use the Schrödinger picture of quantum mechanics and present the postulates connected to this picture.

> **Postulate 1** The system's state is described by a wave function, $\Psi(\tau, t)$, which contains all the system's information.

The wave function describes the state of the system by using quantum numbers. For a hydrogen-like atom, there are five quantum numbers [4].

- The principle quantum number, n: $n = 1, 2, \ldots$
- The angular momentum quantum number, l : $l = 0, \ldots, n-1$
- The magnetic quantum number, m_l: $m_l = -l, \ldots, l$
- The electron spin number, s: $s = \frac{1}{2}$
- The electron spin quantum number, m_s: $m_s = +s, -s$

Each quantum number represents one trait of the system. For an electron in a hydrogen-like atom, the n quantum number represents the energy of the system, and n^2 gives the number of orbitals. The l quantum number represents the angular momentum of the electron and the orbital of the electron. The m_l quantum number describes the shape of the orbital. In addition, there is the

electron spin quantum number which either is spin up, $+\frac{1}{2}$, or spin down $-\frac{1}{2}$. In nonrelativistic quantum mechanics, the spin quantum number was introduced because of Pauli's exclusion principle, which states that the wave function for fermions must be anti-symmetric. In other words, multiple electrons in a hydrogen atom can not have all identical quantum numbers.

Postulate 2 Observables are represented by Hermitian operators chosen to satisfy the following commutation relations, where q is either x, y or z and p_q is the corresponding momentum [4]:

$$\boxed{\begin{array}{ll} \text{(i)} & [q, p_{q'}] = i\hbar\delta_{qq'} \\ \text{(ii)} & [q, q'] = 0 \\ \text{(iii)} & [p_q, p_{q'}] = 0 \end{array}} \tag{2.16}$$

The operators have to be hermitian so that the observables become real.

Postulate 3 When a system is described by Ψ, the mean value of the observable to the operator Ω is known as the expectation value [4].

The expectation value is given by

$$\langle\Omega\rangle = \frac{\langle\Psi|\Omega|\Psi\rangle}{\langle\Psi|\Psi\rangle} \tag{2.17}$$

where $\langle\Psi|\Psi\rangle$ is the overlap integral and is used to normalize the wave function. If Ψ is normalized, $\langle\Psi|\Psi\rangle = 1$, we get

$$\langle\Omega\rangle = \langle\Psi|\Omega|\Psi\rangle. \tag{2.18}$$

If $|\Psi\rangle$ is an eigenfunction of Ω, then $\Omega|\Psi\rangle = \omega|\Psi\rangle$, and the expectation value becomes

$$\langle\Omega\rangle = \omega. \tag{2.19}$$

Now let Ψ be a linear combination of eigenfunctions of Ω

$$\Psi = \sum_n c_n\psi_n \quad \text{where} \quad \Omega|\psi_n\rangle = \omega_n|\psi_n\rangle, \tag{2.20}$$

then

$$\langle\Omega\rangle = \sum_{n,m} c_n c_m^* \langle\psi_m|\Omega|\psi_n\rangle = \sum_{n,m} c_n c_m^* \omega_n \langle\psi_m|\psi_n\rangle. \tag{2.21}$$

Since Ω is hermitian, the eigenfunctions are orthogonal, as stated in postulate 2, which means that the sum can be written as

$$\langle\Omega\rangle = \sum_n c_n c_n^* \omega_n \langle\psi_n|\psi_n\rangle = \sum_n |c_n|^2 \omega_n. \tag{2.22}$$

Here $|c_n|^2$ is the probability of finding the system in the corresponding eigenstate ψ_n [4].

Postulate 4 The probability to find a particle in the volume element $d\tau$ at point $\boldsymbol{r}$ is proportional to $|\Psi(\boldsymbol{r})|^2 d\tau$ [4].

In other words, $|\Psi|^2$ is a probability density. This is often called the Born interpretation, and it implies

$$\int |\Psi|^2 d\tau < \infty. \tag{2.23}$$

For eq.(2.23) to be true, we put a restriction on Ψ [4].

$$\lim_{x \to \pm\infty} \Psi = 0 \tag{2.24}$$

Postulate 5 The wavefunction $\Psi(\tau, t)$ evolves in time according to the equation:

$$i\hbar \frac{\partial \Psi}{\partial t} = H\Psi. \tag{2.25}$$

This is known as the time-dependent Schrödinger equation and is used to evaluate how the system's states changes with time [4].

2.1.3 The Schrödinger equation

The time-dependent Schrödinger equation (TDSE) eq.(2.25) is one of the most essential and fundamental equations in quantum mechanics. Here the H is known as the Hamiltonian operator and consists of two parts, the kinetic energy operator, T, and the potential energy operator, V,

$$H = T + V. \tag{2.26}$$

When H acts on a state, Ψ, it gives the total energy of the system [4]. Here

$$T = \frac{\hat{p}^2}{2m} \quad \text{and} \quad V = V(\boldsymbol{r}). \tag{2.27}$$

$$H_{SE} = \frac{\boldsymbol{p}^2}{2m} + V(\boldsymbol{r}) \tag{2.28}$$

The Schrödinger equation is a second-order partial differential equation and can only be solved analytically for the most straightforward systems. We usually must apply numerical methods to approximate a solution to more complex systems.

The time-independent Schrödinger equation

The Schrödinger equation can be separated into a time-dependent and time-independent part as long as the potential only depends on space (no time dependency). If we start with the time-dependent Schrödinger equation in 1D, we get

$$H_{SE}\Psi = -\frac{1}{2m}\frac{\partial^2 \Psi}{\partial x^2} + V(x)\Psi = i\hbar \frac{\partial \Psi}{\partial t}. \tag{2.29}$$

Using the separation of variables method, we define

$$\Psi(x, t) = \psi(x)\theta(t), \tag{2.30}$$

and obtain

$$-\frac{1}{2m}\theta\frac{\partial^2\psi}{\partial x^2} + V(x)\psi\theta = i\hbar\psi\frac{\partial\theta}{\partial t}.$$

Dividing both sides with Ψ and we get

$$-\frac{1}{2m}\frac{1}{\psi}\frac{\partial^2\psi}{\partial x^2} + V(x) = i\hbar\frac{1}{\theta}\frac{\partial\theta}{\partial t}.$$

Now we see that the right-hand and left-hand sides are independent of each other. Therefore each side must be equal to the same constant. Let us call it E. With this, we get two differential equations,

$$-\frac{1}{2m}\frac{1}{\psi}\frac{\partial^2\psi}{\partial x^2} + V(x) = E, \tag{2.31}$$

and

$$i\hbar\frac{1}{\theta}\frac{\partial\theta}{\partial t} = E. \tag{2.32}$$

Eq.(2.32) can be rewritten as

$$i\hbar\frac{\partial\theta}{\partial t} = E\theta. \tag{2.33}$$

The general solution for θ then becomes

$$\theta(t) = e^{-iEt/\hbar}, \tag{2.34}$$

and eq.(2.31) can take the form

$$H\psi = E\psi. \tag{2.35}$$

This equation is known as the time-independent Schrödinger equation (TISE).

The time part of the wavefunction, $\theta(t)$, can be expressed as a function of sinus and cosines functions through Euler's relation, $e^{ix} = \cos x + i\sin x$,

$$e^{-iEt/\hbar} = \cos Et/\hbar - i\sin Et/\hbar. \tag{2.36}$$

This means that Ψ oscillates between real and imaginary values with time. Even though Ψ oscillates with time for a given energy E, if Ψ is an eigenfunction of H, the probability density of $\Psi^*\Psi$ remains real and constant,

$$\Psi^*\Psi = (\psi^* e^{iEt/\hbar})(\psi e^{-iEt/\hbar}) = \psi^*\psi. \tag{2.37}$$

Therefore, as long as Ψ is an eigenfunction of H, we have a stationary system [4].

2.2 Relativistic Quantum Mechanics

As stated earlier, classical mechanics cannot describe systems moving at relativistic speeds, and we need to apply the theory of relativity. Therefore, to be able to study molecular systems moving with relativistic speeds, we are required to apply relativistic quantum mechanics. Henceforth, we will discuss special relativity, the Dirac equation (the relativistic quantum mechanics equivalent of the Schrödinger equation), and its nonrelativistic limit.

2.2.1 Special relativity

At the beginning of the 20th century, Albert Einstein developed the theory of special relativity, where he described how speed affects time, mass, and space experienced by an observer moving at relativistic speeds [18]. As for quantum mechanics, the theory of special relativity is based on postulates. The two postulates given by Einstein are:

Postulate 1. The laws of physics is the same in all inertial reference frame [18].

Postulate 2. The speed of light, c, in a vacuum is the same in all inertial reference frames and is independent of the motion of the source [18].

Using this, Einstein formulated the relations for time, mass, and space in a system moving at relativistic speeds (accelerated reference frame) compared to a system in an inertial rest frame. The two reference frames are related through the Lorentz factor,

$$\gamma = \frac{1}{\sqrt{1 - \frac{v^2}{c^2}}}. \tag{2.38}$$

The three relativistic effects are known as:

1. **Relativistic mass increase**

$$m = \gamma m_0, \tag{2.39}$$

where m_0 is the rest mass, i.e., the mass for the particle at rest [18].

2. **Length contraction**

$$l = \frac{l_0}{\gamma}, \tag{2.40}$$

where l_0 is the proper length, i.e., the length measured in the accelerated reference system [18].

3. **Time dilation**

$$\Delta t = \gamma \Delta t_0, \tag{2.41}$$

where t_0 is the proper time, i.e., the time measured in the accelerated reference system [18].

Using the relativistic mass correction and the relativistic momentum, we can rewrite the Lorentz factor as a function of momentum, and we get

$$p^2 = (\gamma m_0 v)^2 \Rightarrow \gamma = \sqrt{1 + \left(\frac{p}{m_0 c}\right)^2}. \tag{2.42}$$

Relativistic Energy

In special relativity, we introduce a concept called the rest energy for a particle. It is the energy the particle will give if it is to be annihilated at rest. The rest energy is given by

$$E = m_0 c^2. \tag{2.43}$$

If the particle is accelerated to relativistic speeds, the relativistic mass increase will take effect, and we get

$$E = \gamma m_0 c^2. \tag{2.44}$$

Manipulating this, we can get an expression for the total energy of the free-moving particle,

$$\begin{aligned} E^2 &= (\gamma m_0 c^2)^2 \\ &= \left(\sqrt{1 + \left(\frac{p}{m_0 c} \right)^2} m_0 c^2 \right)^2 \\ &= m_0^2 c^4 + p^2 c^2. \end{aligned} \tag{2.45}$$

The total energy of a free particle then becomes

$$E = \sqrt{m_0^2 c^4 + p^2 c^2}. \tag{2.46}$$

2.2.2 Dirac equation

The Dirac equation is the relativistic equivalent to the nonrelativistic Schrödinger equation. As the TDSE the time-dependent Dirac equation (TDDE) is given by

$$i \frac{\partial \psi}{\partial t} = H_{DE} \psi, \tag{2.47}$$

but the Dirac Hamiltonian, H_{DE}, is significantly different from the Schrödinger Hamiltonian, H_{SE}. First, the Hamiltonian is supposed to give out the system's energy state. The nonrelativistic energy of a free particle is given by

$$E_k = \frac{p^2}{2m} \tag{2.48}$$

which is of $\mathcal{O}(p^2)$, and therefore corresponds to a second-ordered partial differential equation, while the relativistic energy is given by

$$E = \sqrt{m^2 c^4 + p^2 c^2}, \tag{2.49}$$

which is of $\mathcal{O}(p)$, and therefore corresponds to an first ordered differential equation. Note that in eq.(2.49) and eq.(2.48), and henceforth, $m_0 \to m$.

Another important aspect of the Dirac equation is that we have to consider both the particle and antiparticle. This is represented in the wave function, which for the Dirac equation is a four-component spinor,

$$\Psi(\tau, t) = \begin{bmatrix} \psi_1(\tau, t) \\ \psi_2(\tau, t) \\ \psi_3(\tau, t) \\ \psi_4(\tau, t) \end{bmatrix} \tag{2.50}$$

The four components in the Dirac wavefunction can be divided into two two-component spinors,

$$\Psi(\tau,t)=\begin{bmatrix} g(\tau,t) \\ if(\tau,t) \end{bmatrix}, \tag{2.51}$$

where

$$g(\tau,t)=\begin{bmatrix} \psi_1(\tau,t) \\ \psi_2(\tau,t) \end{bmatrix} \quad \text{and} \quad if(\tau,t)=\begin{bmatrix} \psi_3(\tau,t) \\ \psi_4(\tau,t) \end{bmatrix}. \tag{2.52}$$

Here the $g(\tau,t)$ component represents the particle and the $if(\tau,t)$ represents the antiparticle, and each component in $g(\tau,t)$ and $if(\tau,t)$ represents the two spin states. For a particle, the $g(\tau,t)$ component will dominate and be the more significant component, and for an antiparticle, the $if(\tau,t)$ component will dominate. Since we have to consider both particles and antiparticles, we also must consider the negative energy spectrum corresponding to the antiparticle when solving the Dirac equation.

The H_{DE} is given by

$$H_{DE}=c\boldsymbol{\alpha}\cdot\boldsymbol{p}+\beta mc^2-\mathbb{1}e\phi. \tag{2.53}$$

Through minimal coupling, we let

$$\boldsymbol{p}\rightarrow\boldsymbol{p}+e\boldsymbol{A}, \tag{2.54}$$

where $\boldsymbol{A}$ is the vector potential that represents the electromagnetic field. H_{DE} then becomes

$$H_{DE}=c\boldsymbol{\alpha}\cdot(\boldsymbol{p}+e\boldsymbol{A})+\beta mc^2-\mathbb{1}e\phi. \tag{2.55}$$

Here $\boldsymbol{\alpha}$ and β are 4×4 matrices. The α and β matrices can be chosen at will, provided they satisfy the Clifford algebra:

$$\boxed{\begin{array}{ll} \text{(i)} & \beta^2=\alpha_i^2=\mathbb{1} \\ \text{(ii)} & \operatorname{tr}(\alpha_i)=\operatorname{tr}(\beta)=0 \\ \text{(iii)} & \{\alpha_i,\beta\}=0. \end{array}} \tag{2.56}$$

A common choice for the matrices is

$$\beta=\begin{bmatrix} \mathbb{1} & 0 \\ 0 & -\mathbb{1} \end{bmatrix} \quad \text{and} \quad \alpha_i=\begin{bmatrix} 0 & \sigma_i \\ \sigma_i & 0 \end{bmatrix}, \tag{2.57}$$

where σ_i matrices are the Pauli matrices, given by

$$\sigma_1=\begin{bmatrix} 0 & 1 \\ 1 & 0 \end{bmatrix} \quad , \quad \sigma_2=\begin{bmatrix} 0 & -i \\ i & 0 \end{bmatrix} \quad \text{and} \quad \sigma_3=\begin{bmatrix} 1 & 0 \\ 0 & -1 \end{bmatrix}. \tag{2.58}$$

Note that this is not the only representation that can be used, but it is one of the more commonly used.

2.2.3 The non-relativistic limit of the Dirac equation

To construct the relativistic Schrödinger Hamiltonian, we need to explore the non-relativistic limit of the Dirac equation. Due to the structure of the α_i matrices in H_{DE}, there is a coupling between the g and f components. This causes problems when we try to construct the relativistic Schrödinger equation. To study the non-relativistic limit, we need to decouple the H_{DE}. This can be done with the Foldy-Wouthuysen (FW) transformation [17].

We define the terms containing the α_i matrices as odd since they couple the g and f components, and the terms containing the matrices that do not couple the g and f, such as the β and unitary matrix, as even. By defining

$$o = c\boldsymbol{\alpha} \cdot (\boldsymbol{p} + e\boldsymbol{A}) \quad \text{and} \quad \varepsilon = -\mathbb{1}e\phi, \tag{2.59}$$

where o is categorised as odd and ε is categorised as even, we can express the H_{DE} in eq.(2.55) as

$$H_{DE} = o + \varepsilon + \beta mc^2. \tag{2.60}$$

The FW transformation decouples the g and f components by transforming away all the terms containing odd matrices. We do this with a unitary transformation. The unitary transformation is defined by,

$$\Psi' = e^{+iS}\Psi, \tag{2.61}$$

where S is a hermitian operator [17]. Putting this into eq.(2.47) and we get,

$$i\frac{\partial \Psi'}{\partial t} = \left[e^{+iS}\left(H - i\frac{\partial}{\partial t}\right)e^{-iS}\right]\Psi' = H'\Psi'. \tag{2.62}$$

Thus the H' becomes

$$H' = e^{+iS}He^{-iS} - e^{+iS}\dot{S}e^{-iS}. \tag{2.63}$$

We can evaluate this with the Baker-Campbell Hausdorff formula [2]:

$$\begin{aligned} e^{ia}be^{-ia} = b + \frac{i}{1!}[a,b] + \frac{i^2}{2!}[a,[a,b]] \\ + \frac{i^3}{3!}[a,[a,[a,b]]] + \dots. \end{aligned} \tag{2.64}$$

With this, we can express H' as

$$\begin{aligned} H' = H + i[S,H] - \frac{1}{2}[S,[S,H]] - \frac{i}{6}[S,[S,[S,H]]] \\ + \frac{1}{24}[S,[S,[S,[S,H]]]] + \dots + -\dot{S} - \frac{i}{2}[S,\dot{S}] + \frac{1}{6}[S,[S,\dot{S}]] + \dots. \end{aligned} \tag{2.65}$$

To do the FW transformation, we need to know how each of the terms in H_{DE} interacts with the β matrix. This is why the ε and o terms are so convenient since they commute and anti-commute

with the beta, respectively, i.e.,

$$\boxed{\begin{array}{c}[\beta,\varepsilon]=0\\ \\ \{\beta,o\}=0.\end{array}} \tag{2.66}$$

We want to eliminate the o term, so we need to construct an S which causes

$$i[S,\beta mc^2] = -o, \tag{2.67}$$

therefore [17]

$$S = -\frac{\beta o}{2mc^2}. \tag{2.68}$$

After transforming away all the odd terms, we can express H'_{DE} as

$$H'_{DE} = \beta\left(mc^2 + \frac{o^2}{2mc^2} - \frac{o^4}{8m^3c^6}\right) + \varepsilon - \frac{1}{8m^2c^4}[o,[o,\varepsilon]] - \frac{i}{8m^2c^4}[o,\dot{o}]. \tag{2.69}$$

H'_{DE} then becomes

$$\begin{aligned} H'_{DE} = \beta\left(mc^2 + \frac{(\boldsymbol{p}+e\boldsymbol{A})^2}{2m} - \frac{(\boldsymbol{p}+e\boldsymbol{A})^4}{8m^3c^2}\right) - \mathbb{1}\phi + \frac{e}{2m}\boldsymbol{\sigma}_{4\times4}\cdot\boldsymbol{B} \\ + \frac{e}{4m^2c^2}\boldsymbol{\sigma}_{4\times4}\cdot\boldsymbol{E}\times\boldsymbol{p} + \frac{ie}{8m^2c^2}\boldsymbol{\sigma}_{4\times4}\cdot\nabla\times\boldsymbol{E} + \mathbb{1}\frac{e}{8m^2c^2}\nabla\cdot\boldsymbol{E} + \mathcal{O}\left(\frac{1}{c^3}\right). \end{aligned} \tag{2.70}$$

Here

$$\boldsymbol{E} = -\dot{\boldsymbol{A}} - \nabla\phi \quad \text{and} \quad \boldsymbol{B} = \nabla\times\boldsymbol{A}, \tag{2.71}$$

and

$$\sigma_{4\times4_i} = \begin{bmatrix}\sigma_i & 0\\ 0 & \sigma_i\end{bmatrix}, \tag{2.72}$$

where σ_i is the Pauli matrices and $i = 1,2,3$. The detailed calculation is found in the appendix A.1.

There are only even matrices in eq.(2.70), and the equation is uncoupled to the order of $\mathcal{O}\left(\frac{1}{c^2}\right)$. Therefore, it is now possible to split the Hamiltonian into a relativistic Hamiltonian for a particle,

$$\begin{aligned} H_{FW_P} = mc^2 + \frac{(\boldsymbol{p}+e\boldsymbol{A})^2}{2m} - \frac{(\boldsymbol{p}+e\boldsymbol{A})^4}{8m^3c^2} - e\phi + \frac{e}{2m}\boldsymbol{\sigma}\cdot\boldsymbol{B} \\ + \frac{e}{4m^2c^2}\boldsymbol{\sigma}\cdot\boldsymbol{E}\times\boldsymbol{p} + \frac{ie}{8m^2c^2}\boldsymbol{\sigma}\cdot\nabla\times\boldsymbol{E}, + \frac{e}{8m^2c^2}\nabla\cdot\boldsymbol{E} + \mathcal{O}\left(\frac{1}{c^3}\right), \end{aligned} \tag{2.73}$$

and a relativistic Hamiltonian for an antiparticle,

$$\begin{aligned} H_{FW_{AP}} = -mc^2 - \frac{(\boldsymbol{p}+e\boldsymbol{A})^2}{2m} + \frac{(\boldsymbol{p}+e\boldsymbol{A})^4}{8m^3c^2} - e\phi + \frac{e}{2m}\boldsymbol{\sigma}\cdot\boldsymbol{B} \\ + \frac{e}{4m^2c^2}\boldsymbol{\sigma}\cdot\boldsymbol{E}\times\boldsymbol{p} + \frac{ie}{8m^2c^2}\boldsymbol{\sigma}\cdot\nabla\times\boldsymbol{E} + \frac{e}{8m^2c^2}\nabla\cdot\boldsymbol{E} + \mathcal{O}\left(\frac{1}{c^3}\right). \end{aligned} \tag{2.74}$$

For a non-relativistic system, we do not consider the antimatter. Therefore, we only need to consider the particle part of the Hamiltonian, H_{FW_P}, and subtract the particle's rest energy. The

relativistic Schrödinger Hamiltonian, H_{RSE}, then takes the final form of,

$$\begin{aligned} H_{RSE} = \frac{(\boldsymbol{p}+e\boldsymbol{A})^2}{2m} + V - \frac{(\boldsymbol{p}+e\boldsymbol{A})^4}{8m^3c^2} + \frac{e}{2m}\boldsymbol{\sigma}\cdot\boldsymbol{B} \\ + \frac{e}{4m^2c^2}\boldsymbol{\sigma}\cdot\boldsymbol{E}\times\boldsymbol{p} + \frac{ie}{8m^2c^2}\boldsymbol{\sigma}\cdot\nabla\times\boldsymbol{E}, + \frac{e}{8m^2c^2}\nabla\cdot\boldsymbol{E} \end{aligned} \tag{2.75}$$

where we have utilized the $V = -e\phi$.

We recognize that this can be expressed as the non-relativistic Schrödinger Hamiltonian with a few correction terms. The first correction term in eq.(2.75),

$$H_{mv} = -\frac{(\boldsymbol{p}+e\boldsymbol{A})^4}{8m^3c^2}, \tag{2.76}$$

is caused by the relativistic mass increase. Hence it is known as the mass-velocity term [19]. By Taylor expanding the relativistic energy, given in eq.(2.49), and include the $\boldsymbol{A}$ through minimal coupling,

$$E = \sqrt{m^2c^4 + c^2(\boldsymbol{p}+e\boldsymbol{A})^2}, \tag{2.77}$$

the energy becomes

$$E = mc^2 + \frac{1}{2m}(\boldsymbol{p}+e\boldsymbol{A})^2 - \frac{1}{8m^3c^2}(\boldsymbol{p}+e\boldsymbol{A})^4 + \mathcal{O}\left(\frac{1}{c^3}\right). \tag{2.78}$$

Here we recognize the third term in the Taylor expansion as the first correction term in the H_{RSE} [17].

The second correction term corresponds to the magnetic dipole interaction and couples the spin to the $\boldsymbol{B}$ field. The spin operator can be expressed in terms of the Pauli matrices [4],

$$s_i = \frac{1}{2}\hbar\sigma_i, \tag{2.79}$$

where $i = 1, 2, 3$.

The two next terms are the spin-orbit correction, H_{sp},

$$H_{sp} = +\frac{e}{4m^2c^2}\boldsymbol{\sigma}\cdot\boldsymbol{E}\times\boldsymbol{p} + \frac{ie}{8m^2c^2}\boldsymbol{\sigma}\cdot\nabla\times\boldsymbol{E}, \tag{2.80}$$

and couples spin to orbit [17]. In non-relativistic quantum mechanics, states with the same angular momentum quantum number, l, but with a different spin quantum number, m_s, are degenerate, and the energy states are identical. This is not the case in relativistic quantum mechanics, and the corresponding splitting of the energy levels is caused by spin-orbit coupling [20].

The last correction term is known as the Darwin term, H_D, and it is caused by the zitterbewegung effect, the rapid oscillation of the electron. For a point-like nuclear charge, we can express the Darwin term as [20]

$$H_D = \frac{e}{8m^2c^2}\nabla\cdot\boldsymbol{E} = -\frac{e}{8m^2c^2}\nabla^2\phi = -\frac{4\pi e^2}{8m^2c^2}\delta(\boldsymbol{r}). \tag{2.81}$$

Here the $\delta(\boldsymbol{r})$ is the Dirac delta function which is given by

$$\delta(\boldsymbol{r}) = \begin{cases} \infty & \text{for } \boldsymbol{r} = 0 \\ 0 & \text{for } \boldsymbol{r} \neq 0 \end{cases}, \tag{2.82}$$

where

$$\int_{-\infty}^{\infty} \delta(\boldsymbol{r}) d\tau = 1. \tag{2.83}$$

Since only the s have a non-zero wave function at the origin, only these states are affected by the Darwin term [20].

2.3 The Electromagnetic field

To get a better understanding of how light interacts with matter, we need to know how light behaves. Starting from Maxwell's equations, and by discussing the related gauge transformation, we can describe the behavior of the electromagnetic field. Under a gauge transformation, Maxwell's equations remain the same, i.e., the electromagnetic field is gauge invariant. We will also discuss the semi-classical approximation often used in quantum mechanics. Within the aspect of the semi-classical approximation, it is often sufficient to keep the electromagnetic fields classical even though the momentum and energy of the system are quantized.

2.3.1 Maxwell's equations

Maxwell's equations dictate how the electromagnetic field behaves. Within the context of this thesis, we will focus on the equations in vacuum, which are presented accordingly [21]:

$$\boxed{\begin{aligned} &\text{(i)} && \nabla \cdot \boldsymbol{E} = 0 \\ &\text{(ii)} && \nabla \cdot \boldsymbol{B} = 0 \\ &\text{(iii)} && \nabla \times \boldsymbol{E} = -\tfrac{\partial \boldsymbol{B}}{\partial t} \\ &\text{(iv)} && \nabla \times \boldsymbol{B} = \tfrac{1}{c^2}\tfrac{\partial \boldsymbol{E}}{\partial t}. \end{aligned}} \tag{2.84}$$

Here, $\boldsymbol{E}$ is the electric field, and $\boldsymbol{B}$ is the magnetic field. When the electromagnetic field propagates in space, both the $\boldsymbol{E}(\boldsymbol{r}, t)$ and $\boldsymbol{B}(\boldsymbol{r}, t)$ fields are orthogonal to the propagating direction and each other, i.e., the electromagnetic field in a vacuum is a transverse field.

The electromagnetic field can be described by a vector potential, $\boldsymbol{A}(\boldsymbol{r}, t)$, and a scalar potential, $\phi(\boldsymbol{r}, t)$, where $\boldsymbol{E}(\boldsymbol{r}, t)$ and $\boldsymbol{B}(\boldsymbol{r}, t)$ are given by [21],

$$\boldsymbol{E}(\boldsymbol{r}, t) = -\nabla\phi(\boldsymbol{r}, t) - \frac{\partial \boldsymbol{A}(\boldsymbol{r}, t)}{\partial t} \quad \text{and} \quad \boldsymbol{B}(\boldsymbol{r}, t) = \nabla \times \boldsymbol{A}(\boldsymbol{r}, t). \tag{2.85}$$

From Maxwell's equations, we obtain the wave equation, to which both the electric and magnetic fields and the vector potential must adhere. The wave equation for a vector potential is presented as follows

$$\nabla^2 \boldsymbol{A}(\boldsymbol{r}, t) = \frac{1}{c^2}\frac{\partial^2 \boldsymbol{A}(\boldsymbol{r}, t)}{\partial t^2}. \tag{2.86}$$

2.3.2 Gauge transformation

The advantages of expressing the electromagnetic fields in terms of $\boldsymbol{A}(\boldsymbol{r},t)$ and $\phi(\boldsymbol{r},t)$ is that we can do gauge transformation. Under gauge transformation, [22]

$$\boxed{\begin{aligned} \boldsymbol{A} &\to \boldsymbol{A}' = \boldsymbol{A} + \nabla\chi \\ \phi &\to \phi' = \phi - \tfrac{\partial\chi}{\partial t} \\ \psi &\to \psi' = e^{-\frac{i}{\hbar}q\chi}\psi, \end{aligned}} \tag{2.87}$$

where q is the particle's charge, $\chi(\boldsymbol{r},t)$ is any continuous function in which the first and second derivative is also continuous. The $\boldsymbol{E}$ and $\boldsymbol{B}$ fields remain the same under a gauge transformation. Therefore, we say they are gauge invariant.

2.3.3 Semi-classical approximation

As previously introduced, the electron interacts with an electromagnetic field through minimal coupling. In minimal coupling, we let

$$\boldsymbol{p} \to \boldsymbol{p} + e\boldsymbol{A}. \tag{2.88}$$

Putting this into the H_{SE}, we get

$$H_{SE} = \frac{1}{2m}(\boldsymbol{p} + e\boldsymbol{A})^2 + V. \tag{2.89}$$

Here $\boldsymbol{p}$ is quantized, while $\boldsymbol{A}$ and V remains classical. This is known as the semi-classical approximation. It is possible to use a fully quantized picture with a quantized scalar and vector potential, but this is usually unnecessary. Using a fully quantized picture will only be an advantage if we want to study how each photon interacts with the electron [23].

Using Lagrangian mechanics, we can obtain the H_{SE} in eq.(2.89). Starting with the Lorentz force

$$\boldsymbol{F} = q(\boldsymbol{E} + \boldsymbol{v} \times \boldsymbol{B}), \tag{2.90}$$

where q is the particle's charge. From Lagrangian mechanics, the force can be expressed in terms of the potential of the system U, so this force can be expressed as

$$\boldsymbol{F} = \sum_{i=x,y,z} -\frac{\partial U}{\partial i} + \frac{\mathrm{d}}{\mathrm{d}t}\left(\frac{\partial U}{\partial v_i}\right). \tag{2.91}$$

Writing each component of $\boldsymbol{F}$ out and using the relations in eq. (2.85) we get this expression of U,

$$U = q\phi - q\boldsymbol{v}\cdot\boldsymbol{A}. \tag{2.92}$$

The Lagrangian, L, is given by

$$L = T - U, \tag{2.93}$$

where T is the kinetic energy. L then becomes

$$L = \frac{1}{2}m\boldsymbol{v}^2 - q\phi + q\boldsymbol{v}\cdot\boldsymbol{A}. \tag{2.94}$$

We obtain the classical Hamiltonian from the Lagrangian through the relation

$$\begin{aligned} H &= \boldsymbol{p}\cdot\boldsymbol{v} - L \\ &= \boldsymbol{p}\cdot\boldsymbol{v} - \frac{1}{2}m\boldsymbol{v}^2 - q\boldsymbol{v}\cdot\boldsymbol{A} + q\phi. \end{aligned} \tag{2.95}$$

Through Lagrangian mechanics, we express

$$\boldsymbol{p} = \frac{\partial L}{\partial \boldsymbol{v}} = m\boldsymbol{v} + q\boldsymbol{A}. \tag{2.96}$$

Rewriting this expression in terms of $\boldsymbol{v}$ and obtain

$$\boldsymbol{v} = \frac{1}{m}(\boldsymbol{p} - q\boldsymbol{A}). \tag{2.97}$$

Putting this expression for $\boldsymbol{v}$ into eq.(2.95), H becomes

$$H = \frac{1}{2m}(\boldsymbol{p} - q\boldsymbol{A})^2 + q\phi, \tag{2.98}$$

which we recognise as the H_{SE}.

2.3.4 Constructing a quantized photon field

To evaluate how individual photons interact with the electron, we need to utilize a quantized photon field, $\boldsymbol{A_q}(\boldsymbol{r}, t)$. As for the classical field potential, the quantized field potential has to satisfy the wave equation,

$$\nabla^2\boldsymbol{A_q}(\boldsymbol{r}, t) = \frac{1}{c^2}\frac{\partial^2\boldsymbol{A_q}(\boldsymbol{r}, t)}{\partial t^2}. \tag{2.99}$$

A generalized $\boldsymbol{A_q}$ field potential that satisfies the wave equation can be expressed as

$$\boldsymbol{A_q}(\boldsymbol{r}, t) = -i\sum\sqrt{\frac{\hbar}{2\omega\epsilon_0}}[u_k(\boldsymbol{r})a_k(t) + u_k^*(\boldsymbol{r})a_k^*(t)], \tag{2.100}$$

where the $\boldsymbol{A_q}$ is not quantized yet. Putting eq.(2.100) into the wave equation we obtain the solutions,

$$a_k(t) = a_k e^{-i\omega_k t}, \tag{2.101}$$

$$a_k^*(t) = a_k^* e^{i\omega_k t}, \tag{2.102}$$

and

$$u_k(\boldsymbol{r}) = \hat{\varepsilon}_k\frac{1}{\sqrt{V}}e^{i\boldsymbol{k}_n\cdot\boldsymbol{r}}, \tag{2.103}$$

where $\hat{\varepsilon}_k$ is the polarization vector. To quantize the $\boldsymbol{A_q}$, we introduce the creation and annihilation operators for a photon and let

$$a_k \to \hat{a}_k \quad \text{and} \quad a_k^* \to \hat{a}_k^+, \tag{2.104}$$

where $\hat{a}$ is the annihilation operator and $\hat{a}^+$ is the creation operator and satisfies the following commutation relation [24]:

$$\boxed{\begin{array}{ll} \text{(i)} & [\hat{a}_k, \hat{a}_j^+] = \delta_{kj} \\ \text{(ii)} & [\hat{a}_k^+, \hat{a}_j^+] = 0 \\ \text{(iii)} & [\hat{a}_k, \hat{a}_j] = 0. \end{array}} \tag{2.105}$$

Representing the photon state of the system as a number state, $|n_k\rangle$, where n_k is the number of quantized photons, we can express how the $\hat{a}$ and $\hat{a}^+$ acts on a $|n_k\rangle$,

$$\boxed{\begin{array}{ll} \text{(i)} & \hat{a}_k |n_k\rangle = \sqrt{n_k}\, |n_k - 1\rangle \\ \text{(ii)} & \hat{a}_k^+ |n_k\rangle = \sqrt{n_k + 1}\, |n_k + 1\rangle, \end{array}} \tag{2.106}$$

where $n_k = 0, 1, \ldots, \infty$ It is also useful to know that the annihilation operator, $\hat{a}_k$, acting on the ground state, is always 0,

$$\hat{a}_k |0\rangle = 0 |0\rangle . \tag{2.107}$$

The quantized vector potential then becomes

$$\boldsymbol{A_q}(\boldsymbol{r}, t) = -i \sum_k \sqrt{\frac{\hbar}{2\omega_k \epsilon_0 V}} \hat{\varepsilon}_k [\hat{a}_k e^{-i\omega_k t + i\boldsymbol{k}\cdot\boldsymbol{r}} + \hat{a}_k^+ e^{i\omega_k t - i\boldsymbol{k}\cdot\boldsymbol{r}}]. \tag{2.108}$$

The Electric field, corresponding to the $\boldsymbol{A_q}$ field, can be expressed as,

$$\boldsymbol{E_q}(\boldsymbol{r}, t) = \sum_k \sqrt{\frac{\hbar\omega_k}{2\epsilon_0 V}} \hat{\varepsilon}_k [\hat{a}_k e^{-i\omega_k t + i\boldsymbol{k}\cdot\boldsymbol{r}} - \hat{a}_k^+ e^{i\omega_k t - i\boldsymbol{k}\cdot\boldsymbol{r}}], \tag{2.109}$$

through eq.(2.85). Defining

$$E_0 = \sqrt{\frac{\hbar\omega_k}{2\epsilon_0 V}}, \tag{2.110}$$

the $\boldsymbol{A_q}$ turn into

$$\boldsymbol{A_q}(\boldsymbol{r}, t) = -i \sum_k \frac{E_0}{\omega_k} \hat{\varepsilon}_k [\hat{a}_k e^{-i\omega_k t + i\boldsymbol{k}\cdot\boldsymbol{r}} + \hat{a}_k^+ e^{i\omega_k t - i\boldsymbol{k}\cdot\boldsymbol{r}}]. \tag{2.111}$$

Chapter 3

Methods

3.1 Modeling the 1D system

As stated in the introduction, we will study a one-dimensional system, as if the electron is moving in an extremely thin nanotube [16], within a narrow potential. The thin shape of the corresponding potential suggests that the electron's motion is restricted to 1D. This enables us to utilize the dipole approximation and simplifies the Schrödinger, Dirac, and relativistic Schrödinger equations.

3.1.1 The Electromagnetic field in 1D

When an electron interacts with an electromagnetic field, it will be accelerated by the field. Since the electron's movement is restricted to 1D, it cannot move in the propagation direction, only in the oscillation direction, i.e., parallel with the electric field. Studying the force caused on the electron by the $\boldsymbol{E}$ and $\boldsymbol{B}$ fields, respectively, we get,

$$\boldsymbol{F_E} = -e\boldsymbol{E} \quad \text{and} \quad \boldsymbol{F_B} = -e(\boldsymbol{v} \times \boldsymbol{B}). \tag{3.1}$$

Whereas the $\boldsymbol{F_E}$ acts in the polarisation direction of the $\boldsymbol{E}$ field, i.e., the oscillation direction, the $\boldsymbol{F_B}$ acts perpendicularly to both the oscillation and polarisation directions of the $\boldsymbol{B}$ field, i.e., the propagation direction. The electron is not allowed to move in the direction of propagation, so the electron's interaction with the $\boldsymbol{B}$ field can therefore be neglected. Due to this, we can remove the space dependency from the vector potential entirely and let

$$\boldsymbol{A}(\boldsymbol{r}, t) \to \boldsymbol{A}(t), \tag{3.2}$$

also known as the dipole approximation. When the $\boldsymbol{A}$ only depends on time the $\boldsymbol{B}$ field becomes

$$\boldsymbol{B}(t) = \nabla \times \boldsymbol{A}(t) = 0, \tag{3.3}$$

hence the effects caused by the interaction with the $\boldsymbol{B}$ field is neglected, and we are left with the $\boldsymbol{E}$ field solely.

3.1.2 The 1D Schrödinger equation

The electron's interaction with the electromagnetic field is dictated by the time-dependent Schrödinger equation,

$$i\hbar\frac{\partial\psi}{\partial t} = H_{SE}\psi, \tag{3.4}$$

with the minimal-coupling Schrödinger Hamiltonian, H_{SE}, given by eq.(2.89)

$$H_{SE} = \frac{1}{2m}(\boldsymbol{p} + e\boldsymbol{A})^2 + V(\boldsymbol{r}).$$

Reducing the system to 1D,

$$\begin{aligned} \boldsymbol{r} &\to x \\ \boldsymbol{p} &\to p_x \equiv p \\ \boldsymbol{A} &\to A_x \equiv A, \end{aligned} \tag{3.5}$$

and we are left with

$$H_{SE} = \frac{1}{2m}(p + eA)^2 + V(x). \tag{3.6}$$

We can separate the Hamiltonian, H_{SE}, into a time-independent Hamiltonian, H_0, and a time-dependent interaction Hamiltonian, H_I,

$$H_{SE}(x,t) = H_0(x) + H_I(x,t), \tag{3.7}$$

where

$$H_0 = \frac{p^2}{2m} + V(x) \quad \text{and} \quad H_I = \frac{e}{m}Ap + \frac{e^2}{2m}A^2. \tag{3.8}$$

Here the last term in H_I is only dependent on time due to the dipole approximation and can, therefore, be transformed away utilizing the gauge transformation [25],

$$\begin{aligned} A &\to A' = A + \nabla\chi \\ \phi &\to \phi' = \phi - \tfrac{\partial\chi}{\partial t} \\ \psi &\to \psi' = e^{-\frac{i}{\hbar}q\chi}\psi \end{aligned}$$

with

$$\chi = -\frac{e}{2m}\int_0^t A^2(t')dt'. \tag{3.9}$$

The new Schrödinger Hamiltonian can then be expressed as

$$H_{SE} = \frac{p^2}{2m} + \frac{eAp}{m} + V, \tag{3.10}$$

where

$$H_0 = \frac{p^2}{2m} + V \quad \text{and} \quad H_I = \frac{eAp}{m}. \tag{3.11}$$

3.1.3 The 1D Dirac equation

At relativistic speeds, the electron's interaction with the laser pulse is dictated by the time-dependent Dirac equation,

$$i\hbar\frac{\partial\psi}{\partial t} = H_{DE}\psi, \tag{3.12}$$

with the minimal-coupling Dirac Hamiltonian, H_{DE}, given by eq.(2.55)

$$H_{DE} = c\boldsymbol{\alpha}\cdot(\boldsymbol{p} + e\boldsymbol{A}) + \beta mc^2 - \mathbb{1}e\phi.$$

By reducing the system to 1D, we can perform a simplification on the wavefunction spinor. Since there is no angular momentum in 1D, we may also argue that there is no spin [26]. Some articles treat a relativistic 1D problem as if spin exists [27], and others assume that it does not [26]. Either way, it does not affect the results since the spin couples to the orbit and the $\boldsymbol{B}$ field, as discussed in section 2.2.3, which both require a minimum of 2D. Hence we will approach the problem as if spin can be neglected in 1D.

Since the spin can be neglected, the four-component spinor wavefunction can be reduced to a two-component spinor, and we are left with

$$\psi = \begin{bmatrix} g(x,t) \\ if(x,t) \end{bmatrix}, \tag{3.13}$$

where $g(x,t)$ corresponds to the wavefunction of a particle, and $if(x,t)$ corresponds to the wavefunction of an antiparticle. Because the spinor wavefunction is reduced to two components, we also need to reduce the dimensions on the α and β matrices so they become 2×2 matrices. As we mentioned in section 2.2, the α and β matrices can be chosen at will, provided they satisfy the Clifford algebra, expressed in eq.(2.56),

(i)	$\beta^2 = \alpha^2 = \mathbb{1}$
(ii)	$\mathrm{tr}(\alpha) = \mathrm{tr}(\beta) = 0$
(iii)	$\{\alpha, \beta\} = 0$

We already know a set of 2×2 matrices that satisfy this relation, namely the Pauli matrices expressed in eq.(2.58),

$$\sigma_1 = \begin{bmatrix} 0 & 1 \\ 1 & 0 \end{bmatrix} \quad \text{and} \quad \sigma_2 = \begin{bmatrix} 0 & -i \\ i & 0 \end{bmatrix} \quad \text{and} \quad \sigma_3 = \begin{bmatrix} 1 & 0 \\ 0 & -1 \end{bmatrix}.$$

Here we choose

$$\alpha = \sigma_2 \quad \text{and} \quad \beta = \sigma_3. \tag{3.14}$$

The Dirac Hamiltonian can now be expressed as

$$H_{DE} = c\alpha(p + eA) + \beta mc^2 - \mathbb{1}e\phi. \tag{3.15}$$

As for the Schrödinger Hamiltonian, H_{SE}, we can separate the Dirac Hamiltonian, H_{DE}, into a time-independent Hamiltonian, H_0, and a time-dependent interaction Hamiltonian, H_I,

$$H_{DE}(x,t) = H_0(x) + H_I(x,t), \tag{3.16}$$

where

$$H_0 = c\alpha p + \beta mc^2 - \mathbb{1}e\phi \quad \text{and} \quad H_I = ce\alpha A. \tag{3.17}$$

3.1.4 The 1D relativistic Schrödinger equation

The relativistic electron's interaction with the laser pulse can also approximately be described by the time-dependent relativistic Schrödinger equation, given by,

$$i\hbar\frac{\partial\psi}{\partial t} = H_{RSE}\psi, \tag{3.18}$$

where H_{RSE} was constructed in section 2.2, and is expressed in eq.(2.75),

$$\begin{aligned} H_{RSE} = &\frac{(\boldsymbol{p}+e\boldsymbol{A})^2}{2m} - \frac{(\boldsymbol{p}+e\boldsymbol{A})^4}{8m^3c^2} + V + \frac{e}{2m}\boldsymbol{\sigma}\cdot\boldsymbol{B} \\ &+ \frac{e}{4m^2c^2}\boldsymbol{\sigma}\cdot\boldsymbol{E}\times\boldsymbol{p} + \frac{ie}{8m^2c^2}\boldsymbol{\sigma}\cdot\nabla\times\boldsymbol{E} + \frac{e}{8m^2c^2}\nabla\cdot\boldsymbol{E}. \end{aligned} \tag{3.19}$$

The H_{RSE} was constructed utilizing the FW transformation on the 3D Dirac equation. To construct the 1D H_{RSE}, we do the same for the 1D Dirac equation. The 1D Dirac Hamiltonian is given in eq.(3.15), and by defining

$$o = c\alpha(p + eA) \quad \text{and} \quad \varepsilon = -\mathbb{1}e\phi, \tag{3.20}$$

where o is the odd terms and ε is the even terms, we can rewrite H_{DE} as

$$H_{DE} = o + \varepsilon + \beta mc^2. \tag{3.21}$$

Doing the same procedure as in section 2.2.3 the FW transformation produces a H'_{DE} as given in eq.(2.69),

$$H'_{DE} = \beta\left(mc^2 + \frac{o^2}{2mc^2} - \frac{o^4}{8m^3c^6}\right) + \varepsilon - \frac{1}{8m^2c^4}[o,[o,\varepsilon]] - \frac{i}{8m^2c^4}[o,\dot{o}]. \tag{3.22}$$

The H'_{DE} then becomes

$$H'_{DE} = \beta\left(mc^2 + \frac{(p+eA)^2}{2m} - \frac{(p+eA)^4}{8m^3c^2}\right) + \mathbb{1}V + \mathbb{1}\frac{1}{8m^2c^2}\frac{\partial^2 V}{\partial x^2}. \tag{3.23}$$

The derivation is found in appendix A.2. The H'_{DE} only contains even matrices and can be separated into a Hamiltonian for the particle,

$$H_{FW_P} = mc^2 + \frac{(p+eA)^2}{2m} - \frac{(p+eA)^4}{8m^3c^2} + V + \frac{1}{8m^2c^2}\frac{\partial^2 V}{\partial x^2} \tag{3.24}$$

and a Hamiltonian for the antiparticle,

$$H_{FW_{AP}} = -mc^2 - \frac{(p+eA)^2}{2m} + \frac{(p+eA)^4}{8m^3c^2} + V + \frac{1}{8m^2c^2}\frac{\partial^2 V}{\partial x^2}. \tag{3.25}$$

As previously stated, the Schrödinger equation does not consider anti-matter. Therefore we can construct the 1D relativistic Schrödinger Hamiltonian, H_{RSE}, by subtracting the rest energy, mc^2, from the H_{FW_P}. The H_{RSE} then becomes

$$H_{RSE} = \frac{(p+eA)^2}{2m} - \frac{(p+eA)^4}{8m^3c^2} + V + \frac{1}{8m^2c^2}\frac{\partial^2 V}{\partial x^2}. \tag{3.26}$$

Comparing eq.(3.19) and eq.(3.26) we see that in 1D, the spin-orbit terms and the magnetic dipole term are eliminated. As stated in section 2.2.3, the spin-orbit terms are what is causing the split in the energy levels in terms of spin. The absence of these terms in the 1D H_{RSE} further strengthens the assumption that we do not need to consider the spin when solving the 1D Dirac equation. We are left with the mass-velocity term

$$H_{mv} = -\frac{(p+eA)^4}{8m^3c^2}, \tag{3.27}$$

and we have expressed the Darwin term in terms of the Coulomb potential,

$$H_D = \frac{1}{8m^2c^2}\frac{\partial^2 V}{\partial x^2}. \tag{3.28}$$

As for the H_{SE} and H_{DE}, the H_{RSE} can be separated into a time-independent Hamiltonian, H_0, and a time-dependent interaction Hamiltonian, H_I,

$$H_{RSE}(x,t) = H_0(x) + H_I(x,t). \tag{3.29}$$

Here

$$H_0 = \frac{p^2}{2m} - \frac{p^4}{8m^3c^2} + V + \frac{1}{8m^2c^2}\frac{\partial^2 V}{\partial x^2} \tag{3.30}$$

and

$$H_I = \frac{e}{m}Ap + \frac{e^2}{2m}A^2 - \frac{e}{2m^3c^2}Ap^3 - \frac{3e^2}{4m^3c^2}A^2p^2 - \frac{e^3}{2m^3c^2}A^3p - \frac{e^4}{8m^3c^2}A^4, \tag{3.31}$$

where again the terms $\frac{e^2}{2m}A^2$ and $-\frac{e^4}{8m^3c^2}A^4$ are only dependent on time. This enables us to utilize a gauge transformation to eliminate these terms, as we did for the Schrödinger equation [25]. The relativistic Schrödinger Hamiltonian, H_{RSE}, then becomes

$$H_{RSE} = \frac{p^2}{2m} - \frac{p^4}{8m^3c^2} + V + \frac{1}{8m^2c^2}\frac{\partial^2 V}{\partial x^2} + \frac{e}{m}Ap \underbrace{- \frac{e}{2m^3c^2}Ap^3 - \frac{3e^2}{4m^3c^2}A^2p^2 - \frac{e^3}{2m^3c^2}A^3p}_{\text{Term } I}, \tag{3.32}$$

where the term I is the transient relativistic effect.

3.2 The time-independent system

Related back to, the above-stated; the 1D system can be thought of as if the electron is moving inside a nanotube within a narrow potential. This can be modeled as a 1D particle-in-box problem with a soft-coulomb potential. The advantage of basing the model on a 1D particle-in-box problem is that we can utilize their analytical solution as a basis for solving the time-independent Schrödinger equation (TISE), the time-independent relativistic Schrödinger equation (TIRSE), and the time-independent Dirac equation (TIDE). The particle-in-box basis for a box defined from $x \in [0, L]$ is given by

$$\varphi_n = \sqrt{\frac{2}{L}} \sin\Big(\frac{\pi n}{L} x\Big), \tag{3.33}$$

where $n = 1, 2, 3, \ldots$. We can express the wavefunction of the system as a linear combination of the particle-in-box basis functions,

$$|\psi\rangle = \sum_n c_n |\varphi_n\rangle. \tag{3.34}$$

By solving the time-independent system as the eigenvalue problem,

$$H|\psi\rangle = E|\psi\rangle, \tag{3.35}$$

we can construct the eigenstates and the corresponding eigenvalues of the potential.

3.2.1 Solving the TISE and TIRSE

Starting with eq.(3.35), and by expressing the wavefunction as in eq.(3.34), we acquire the equation

$$H \sum_{n=1}^{N} c_n |\varphi_n\rangle = E \sum_{n=1}^{N} c_n |\varphi_n\rangle, \tag{3.36}$$

where $n = 1, 2, 3, \ldots, N$ and N is the number of basis functions. By multiplying eq.(3.36) with $\langle\varphi_m|$ from the left this becomes

$$\sum_{n=1}^{N} c_n \langle\varphi_m|H|\varphi_n\rangle = E \sum_{n=1}^{N} c_n \langle\varphi_m|\varphi_n\rangle, \tag{3.37}$$

where $m = 1, 2, 3, \ldots, N$. As discussed in section 2.1 the $\langle\varphi_m|H|\varphi_n\rangle$ and $\langle\varphi_m|\varphi_n\rangle$ can be considered a matrix element in the $\boldsymbol{H}$ and $\boldsymbol{S}$ matrices. Therefore, we can express

$$\langle\varphi_m|H|\varphi_n\rangle = \boldsymbol{H_{mn}} \quad \text{and} \quad \langle\varphi_m|\varphi_n\rangle = \boldsymbol{S_{mn}}. \tag{3.38}$$

Another advantage of the particle-in-box basis is that it is orthogonal, which causes the overlap matrix, $\boldsymbol{S}$, to become the identity matrix, $\mathbb{1}$, expressed mathematically as

$$\boldsymbol{S_{mn}} = \langle\varphi_m|\varphi_n\rangle = \delta_{mn} \Rightarrow \boldsymbol{S} = \mathbb{1}. \tag{3.39}$$

Eq.(3.37) can then be expressed as

$$\sum_{n=1}^{N} c_n \boldsymbol{H_{mn}} = E \sum_{n=1}^{N} c_n \delta_{mn}. \tag{3.40}$$

This can also be expressed as a matrix equation,

$$\begin{bmatrix} \boldsymbol{H_{11}} & \boldsymbol{H_{12}} & \cdots & \boldsymbol{H_{1N}} \\ \boldsymbol{H_{21}} & \boldsymbol{H_{22}} & \cdots & \boldsymbol{H_{2N}} \\ \vdots & \vdots & \ddots & \vdots \\ \boldsymbol{H_{N1}} & \boldsymbol{H_{N2}} & \cdots & \boldsymbol{H_{NN}} \end{bmatrix} \begin{bmatrix} c_1 \\ c_2 \\ \vdots \\ c_N \end{bmatrix} = E \begin{bmatrix} 1 & 0 & \cdots & 0 \\ 0 & 1 & \cdots & 0 \\ \vdots & \vdots & \ddots & \vdots \\ 0 & 0 & \cdots & 1 \end{bmatrix} \begin{bmatrix} c_1 \\ c_2 \\ \vdots \\ c_N \end{bmatrix}, \tag{3.41}$$

or

$$\boldsymbol{Hc} = \mathbb{1} E \boldsymbol{c}, \tag{3.42}$$

where $\boldsymbol{c}$ is a vector with N components and $\boldsymbol{H}$ is a $N \times N$ matrix. We solve this matrix equation as an eigenvalue problem. This is done by diagonalizing the $\boldsymbol{H}$ matrix. Through the diagonalization procedure, we construct two matrices, $\boldsymbol{P}$ and $\boldsymbol{D}$, which relates to the $\boldsymbol{H}$ matrix as

$$\boldsymbol{H} = \boldsymbol{P}^{-1} \boldsymbol{D} \boldsymbol{P}. \tag{3.43}$$

The $\boldsymbol{D}$ matrix is a diagonal matrix where each matrix element, $\boldsymbol{D_{mm}}$, corresponds to an eigenvalue, λ_m, or energy state, of the system. The $\boldsymbol{P}$ matrix consist of the corresponding eigenvectors, $\boldsymbol{c_m}$, where each coulomb represents one eigenvector,

$$\boldsymbol{P} = [\boldsymbol{c_1}, \boldsymbol{c_2}, \cdots, \boldsymbol{c_N}], \tag{3.44}$$

and the eigenvector $\boldsymbol{c_m}$ corresponds to the eigenvalue λ_m. Each vector element in $\boldsymbol{c_m}$ represents one coefficient, c_n, in eq.(3.34) and we can then express the eigenstates as

$$|\psi_m\rangle = \sum_{n=1}^{N} c_{m_n} |\varphi_n\rangle, \tag{3.45}$$

where $m = 1, 2, \ldots, N$.

3.2.2 Solving the TIDE

Solving the TIDE is very similar to solving the TISE and TIRSE. Still, due to the Dirac wavefunction being a two-component spinor, we need to modify the particle-in-box basis. We do this by utilizing dual kinetic balance (DKB), which also eliminates ghost states [28]. Ghost states are, in this case, unreal energy states with a negative norm (negative probability) and often occur when solving the Dirac eigenvalue problem and when we use quantum field theory [28, 29, 30].

Dual kinetic balance

When solving the TIDE eigenvalue problem, we must consider both the positive energy states corresponding to a particle and the negative energy states corresponding to an antiparticle. Therefore the basis for the TIDE must be twice as large as for the TISE and TIRSE. Hence, the Dirac

Hamiltonian matrix becomes a $2N \times 2N$ matrix. Expressing the Dirac Hamiltonian, eq.(3.17), as a matrix,

$$H_{DE} = \begin{bmatrix} mc^2 + V & -c\frac{\partial}{\partial x} \\ c\frac{\partial}{\partial x} & -mc^2 + V \end{bmatrix}, \tag{3.46}$$

allows us to utilize DKB to construct a 1D two-component spinor basis for the TIDE [28]. By defining the spinor basis as

$$\varphi_n(x) = \begin{bmatrix} g_n(x) \\ f_n(x) \end{bmatrix}, \tag{3.47}$$

we can express the wavefunction, $|\psi\rangle$, as a liner combination of $|\varphi_n\rangle$, and obtain

$$|\psi\rangle = \sum_{n=1}^{2N} c_n |\varphi_n\rangle, \tag{3.48}$$

where

$$\varphi_n = \begin{bmatrix} g_n(x) \\ f_n(x) \end{bmatrix} \tag{3.49}$$

and $n = 1, 2, 3, \ldots, 2N$.

Through DKB, we define the relationship between the particle and antiparticle components as follows [28],

$$\varphi_n(x) = \begin{bmatrix} g_n(x) \\ f_n(x) \end{bmatrix} = \begin{bmatrix} u_n(x) \\ \frac{1}{2mc} u_n(x) \end{bmatrix} \quad n \in [1, N], \tag{3.50}$$

and

$$\varphi_n(x) = \begin{bmatrix} g_n(x) \\ f_n(x) \end{bmatrix} = \begin{bmatrix} \frac{1}{2mc} u_{(n-N)}(x) \\ u_{(n-N)}(x) \end{bmatrix} \quad n \in [1 + N, 2N]. \tag{3.51}$$

Again, we choose to use the 1D particle-in-box basis as $u_n(x)$, and is given by

$$u_n(x) = \sqrt{\frac{2}{L}} \sin\Big(\frac{\pi n}{L} x\Big), \tag{3.52}$$

where $n = 1, 2, 3, \ldots, N$. Henceforth, this will be used as the basis for the TIDE and will be known as the DKB basis.

The TIDE eigenvalue problem

We solve the TIDE eigenvalue problem similar to the TISE and TIRSE eigenvalue problems. However, the DKB basis is not orthogonal,

$$\boldsymbol{S_{mn}} = \langle \varphi_m | \varphi_n \rangle \neq \delta_{mn}, \tag{3.53}$$

so the matrix equation becomes

$$\begin{bmatrix} \boldsymbol{H_{11}} & \boldsymbol{H_{12}} & \cdots & \boldsymbol{H_{1\,2N}} \\ \boldsymbol{H_{21}} & \boldsymbol{H_{22}} & \cdots & \boldsymbol{H_{2\,2N}} \\ \vdots & \vdots & \ddots & \vdots \\ \boldsymbol{H_{2N\,1}} & \boldsymbol{H_{2N\,2}} & \cdots & \boldsymbol{H_{2N\,2N}} \end{bmatrix} \begin{bmatrix} c_1 \\ c_2 \\ \vdots \\ c_{2N} \end{bmatrix} = E \begin{bmatrix} \boldsymbol{S_{11}} & \boldsymbol{S_{12}} & \cdots & \boldsymbol{S_{1\,2N}} \\ \boldsymbol{S_{21}} & \boldsymbol{S_{22}} & \cdots & \boldsymbol{S_{2\,2N}} \\ \vdots & \vdots & \ddots & \vdots \\ \boldsymbol{S_{2N\,1}} & \boldsymbol{S_{2N\,2}} & \cdots & \boldsymbol{S_{2N\,2N}} \end{bmatrix} \begin{bmatrix} c_1 \\ c_2 \\ \vdots \\ c_{2N} \end{bmatrix}, \tag{3.54}$$

or in its compact form

$$\boldsymbol{H}\boldsymbol{c} = E\boldsymbol{S}\boldsymbol{c}. \tag{3.55}$$

$\boldsymbol{H}$ and $\boldsymbol{S}$ are both of dimensions $2N \times 2N$ and can be divided into four sub-matrices, α, β, γ and δ,

$$\boldsymbol{H} = \begin{bmatrix} \boldsymbol{H}^{[\alpha]} & \vdots & \boldsymbol{H}^{[\beta]} \\ \cdots & \ddots & \cdots \\ \boldsymbol{H}^{[\gamma]} & \vdots & \boldsymbol{H}^{[\delta]} \end{bmatrix} \quad \text{and} \quad \boldsymbol{S} = \begin{bmatrix} \boldsymbol{S}^{[\alpha]} & \vdots & \boldsymbol{S}^{[\beta]} \\ \cdots & \vdots & \cdots \\ \boldsymbol{S}^{[\gamma]} & \vdots & \boldsymbol{S}^{[\delta]} \end{bmatrix}. \tag{3.56}$$

Each sub-matrix has the dimension $N \times N$. The α sub-matrices are defined for $j \in [1, N]$ and $i \in [1, N]$, where i is the initial state and j is the final state. The β sub-matrices are defined for $j \in [1, N]$ and $i \in [1 + N, 2N]$, the γ sub-matrices are defined for $j \in [1 + N, 2N]$ and $i \in [1, N]$, and the δ sub-matrices are defined for $j \in [1 + N, 2N]$ and $i \in [1 + N, 2N]$. The DKB basis for each of the sub-matrices is given in the tab. 3.1.

$\boldsymbol{\alpha}$			$\boldsymbol{\beta}$		
	$g_{j/i}$	$f_{j/i}$		$g_{j/i}$	$f_{j/i}$
$j \in [1, N]$	$\sqrt{\frac{2}{L}} \sin \frac{\pi j}{L} x$	$\frac{1}{2mc} \frac{\mathrm{d}g_j}{\mathrm{d}x}$	$j \in [1, N]$	$\sqrt{\frac{2}{L}} \sin \frac{\pi j}{L} x$	$\frac{1}{2mc} \frac{\mathrm{d}g_j}{\mathrm{d}x}$
$i \in [1, N]$	$\sqrt{\frac{2}{L}} \sin \frac{\pi i}{L} x$	$\frac{1}{2mc} \frac{\mathrm{d}g_i}{\mathrm{d}x}$	$i \in [1 + N, 2N]$	$\frac{1}{2mc} \frac{\mathrm{d}f_i}{\mathrm{d}x}$	$\sqrt{\frac{2}{L}} \sin \frac{\pi (i-N)}{L} x$
$\boldsymbol{\gamma}$			$\boldsymbol{\delta}$		
	$g_{j/i}$	$f_{j/i}$		$g_{j/i}$	$f_{j/i}$
$j \in [1 + N, 2N]$	$\frac{1}{2mc} \frac{\mathrm{d}f_j}{\mathrm{d}x}$	$\sqrt{\frac{2}{L}} \sin \frac{\pi (j-N)}{L} x$	$j \in [1 + N, 2N]$	$\frac{1}{2mc} \frac{\mathrm{d}f_j}{\mathrm{d}x}$	$\sqrt{\frac{2}{L}} \sin \frac{\pi (j-N)}{L} x$
$i \in [1, N]$	$\sqrt{\frac{2}{L}} \sin \frac{\pi i}{L} x$	$\frac{1}{2mc} \frac{\mathrm{d}g_i}{\mathrm{d}x}$	$i \in [1 + N, 2N]$	$\frac{1}{2mc} \frac{\mathrm{d}f_i}{\mathrm{d}x}$	$\sqrt{\frac{2}{L}} \sin \frac{\pi (i-N)}{L} x$

Table 3.1: The DKB basis for each of the sub-matrices

When the $\boldsymbol{H}$ and $\boldsymbol{S}$ matrices are constructed, we solve the eigenvalue problem similarly as we did for the TISE and the TIRSE. The only difference is that since the DKB basis is not orthogonal and the $\boldsymbol{S} \neq \mathbb{1}$. Hence we need to multiply eq.(3.55) with $\boldsymbol{S}^{-1}$ form the left,

$$\boldsymbol{S}^{-1}\boldsymbol{H}\boldsymbol{c} = E\mathbb{1}\boldsymbol{c}, \tag{3.57}$$

and diagonalize the $\boldsymbol{S}^{-1}\boldsymbol{H}$. As for the TISE and TIRSE, the diagonalization process produces two matrices, $\boldsymbol{P}$ and $\boldsymbol{D}$, and are related to $\boldsymbol{S}^{-1}\boldsymbol{H}$ though

$$\boldsymbol{S}^{-1}\boldsymbol{H} = \boldsymbol{P}^{-1}\boldsymbol{D}\boldsymbol{P}. \tag{3.58}$$

The $\boldsymbol{P}$ matrix is utilized, as for the TISE and the TIRSE, to construct the TIDE eigenvalue basis. The $\boldsymbol{P}$ matrix is defined in eq.(3.44),

$$\boldsymbol{P} = [\boldsymbol{c_1}, \boldsymbol{c_2}, \cdots, \boldsymbol{c_N}],$$

where each $\boldsymbol{c}_m$ represent one eigenvector. We can, therefore, express the wavefunction as,

$$|\psi_m\rangle = \sum_{n=1}^{2N} c_{m_n} |\varphi_n\rangle, \tag{3.59}$$

where $m = 1, 2, 3, \ldots, 2N$. We define this as the eigenvalue basis for the Dirac equation.

3.2.3 Gauss-Lagrange quadrature

To calculate the $\boldsymbol{H_{mn}}$ and $\boldsymbol{S_{mn}}$ matrix elements we need to evaluate an the integrals

$$\boldsymbol{H_{mn}} = \langle \varphi_m | \, H \, | \varphi_n \rangle = \int \varphi_m^* H \varphi_n d\tau \tag{3.60}$$

and

$$\boldsymbol{S_{mn}} = \langle \varphi_m | \varphi_n \rangle = \int \varphi_m^* \varphi_n d\tau. \tag{3.61}$$

The soft coulomb potential in H makes it difficult to calculate these integrals analytically, so applying a numerical method is beneficial.

The numerical method in question is known as the Gauss-Lagrange quadrature (GL). The GL theorem states that an integral of a polynomial of order $2n-1$ can be solved exactly with a sum over n points, x_i, and the n corresponding weight, w_i [31]. The GL theorem in mathematical form writes as follows,

$$\int_{-1}^{1} f(x)\, dx = \sum_{i=1}^{n} w_i f(x_i). \tag{3.62}$$

Here the integral is defined for $x \in [-1, 1]$. Our model is based on a particle-in-box, where $x \in [0, L]$. Hence we need to change the integration limits. This is possible by doing a translation. Starting with

$$\int_a^b f(x)\, dx = \int_{-1}^{1} f(u)\, du \tag{3.63}$$

By doing a translation, we define

$$x = mu + c. \tag{3.64}$$

Which allows us to express the interaction limits a and b in terms of u,

$$a = m(-1) + c \quad \text{and} \quad b = m(+1) + c. \tag{3.65}$$

Now, manipulating this set of equations, we can express m and c in terms of a and b,

$$m = \frac{b-a}{2} \quad \text{and} \quad c = \frac{b+a}{2}. \tag{3.66}$$

x can then be expressed as

$$x = \frac{b-a}{2}u + \frac{b+a}{2}, \tag{3.67}$$

and dx becomes

$$dx = \frac{b-a}{2} du. \tag{3.68}$$

In our model, both the particle-in-box and DKB basis are based on sinus functions, a polynomial of infinite order. Hence the GL is quite a good approximation. The integral, with $a = 0$ and $b = L$, then becomes

$$\int_a^b f(x)\, dx = \int_{-1}^{1} f\left(\frac{L}{2}u + \frac{L}{2}\right)\left(\frac{L}{2}\right) du \approx \left(\frac{L}{2}\right) \sum_{i=1}^{n} w_i f\left(\frac{L}{2}u_i + \frac{L}{2}\right). \tag{3.69}$$

We compute the nodes and weights using the Matlab script **lglnodes.m** [32].

3.2.4 Energy state correction for the time-independent system

The time-independent problem is modeled by the 1D particle-in-box problem with a soft-Coulomb potential, shown in fig. 3.1. We choose to use a 1D soft-coulomb potential in contrast to a

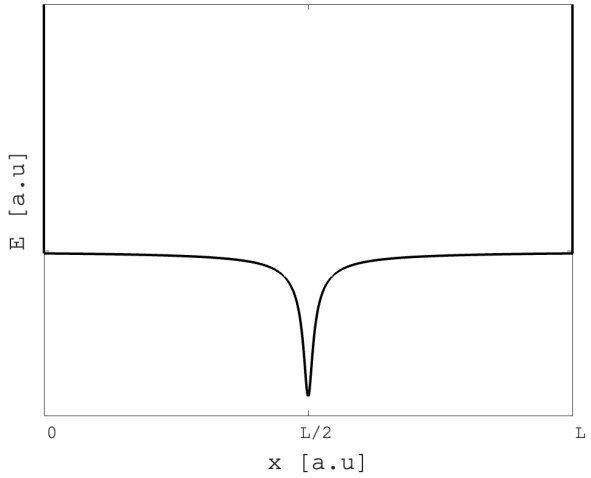

Figure 3.1: Particle-in-box with a soft Coulomb potential.

proper-coulomb potential to get the correct ground state energy for the 1D hydrogen-like atom,

$$V(x) = -\frac{Z}{\sqrt{(x-\frac{L}{2})^2+\frac{2}{Z^2}}}. \tag{3.70}$$

We solve this 1D time-independent problem, by solving the TISE, TIDE, and TIRSE utilizing MatLab. Choosing to study a hydrogen-like Boron atom, i.e., we set $Z = 5$ in eq.(3.70), we investigate the relativistic corrections to the Boron atom's energy states.

	Energy [a.u]			Relativistic correction [10^{-5}a.u]	
State (n)	TISE	TIRSE	TIDE	TIRSE	TIDE
1	−12.5000000	−12.4999409	−12.4999408	5.91	5.92
2	−5.8225834	−5.8232056	−5.8232054	−62.22	−62.22
3	−3.3457215	−3.3461079	−3.3461078	−38.64	−38.63

Table 3.2: Energy levels for $n = 1$ to $n = 3$ for TISE, TIRSE, and TIDE, and their respective relativistic corrections.

The relativistic energy corrections for the 1D system are quite small, in contrast to what would be expected from a 3D system. The relativistic corrections for $n = 1, 2, 3$ are given in the tab. 3.2. By comparing the correction of the ground state energy in 1D to the 3D correction, as shown in tab. 3.3, we observe that the 1D correction is also in the opposite direction than we expected.

To help better understand why this is the case, we would like to study the effect of each individual correction term in the time-independent H_{RSE} eq.(3.30) when solving the TIRSE. In

	Energy [a.u]			Relativistic correction [10^{-5}a.u]	
State (n)	TISE	TIDE (3D)	TIDE (1D)	TIDE (3D)	TIDE (1D)
1	−12.5000000	−12.52086	−12.4999408	−2086	5.92

Table 3.3: Ground state energy for the TISE, the 3D TIDE and the the 1D TIDE. The 3D data is from [33].

the time-independent H_{RSE}, eq.(3.30), there are only two correction terms, the mass-velocity term,

$$H_{mv} = -\frac{p^4}{8m^3c^2}, \tag{3.71}$$

and the Darwin term,

$$H_D = \frac{1}{8m^2c^2}\frac{\partial^2 V}{\partial x^2}. \tag{3.72}$$

The relativistic correction for each term is given in the tab. 3.4, for $n = 1, 2, 3$. Here it becomes

	Energy [a.u]			Relativistic correction [10^{-5}a.u]		
State (n)	TISE	TIRSE$_{MV}$	TIRSE$_D$	TIRSE$_{MV}$	TIRSE$_D$	TIRSE
1	−12.5000000	−12.5003446	−12.4995964	−34.46	40.36	5.91
2	−5.8225834	−5.8230666	−5.8227225	−48.31	−13.91	−62.22
3	−3.3457215	−3.3460987	−3.3457307	−37.72	−0.93	−38.64

Table 3.4: Energy levels for $n = 1$ to $n = 3$ for TISE, TIRSE$_{MV}$, TIRSE$_D$ and TIRSE and each contribution to the relativistic correction.

apparent that for the ground state, the Darwin correction and the mass-velocity correction are of the same magnitude, but in opposite directions, with the Darwin correction being slightly larger. We observe that the mass-velocity therm produces the most important correction for higher energies. In section 2.2.3 and eq.(2.81) we mentioned how we could express the 3D Darwin term for a point charge as

$$H_D = \frac{e}{8m^2c^2}\nabla \cdot \boldsymbol{E} = -\frac{4\pi e^2}{8m^2c^2}\delta(\boldsymbol{r}).$$

For higher energies, the electron is farther away from the nucleus. Hence the Darwin therm becomes less contributing.

In 3D, the relatively large correction is caused by the $\boldsymbol{p}^4$ in the 3D H_{mv}, eq.(2.76) [34]. The difference in the relativistic correction for a system in 1D compared to a 3D system can, therefore, be explained by the difference in the momentum. In a 3D system, we utilize a proper-coulomb potential

$$V_{3D} = -\frac{Z}{r}, \tag{3.73}$$

where r is the radial coordinate in spherical coordinates. While in the 1D system, we utilize a soft-coulomb potential, expressed in eq.(3.70). The virtual theorem states that for a potential that can be expressed as

$$V = ax^s, \tag{3.74}$$

the kinetic energy and potential energy are related through [4],

$$2\langle E_k \rangle = s\langle E_p \rangle. \tag{3.75}$$

For the proper-coulomb potential $s = -1$, and utilizing the virtual theorem, we can express the electron's momentum in the ground state as a function of the ground state energy, E_g. The ground state energy can be expressed as

$$E_g = \langle E_k \rangle + \langle E_p \rangle = \left(1 + \frac{2}{-1}\right) \langle E_k \rangle = -\langle E_k \rangle, \tag{3.76}$$

then the momentum becomes

$$p = \sqrt{-2mE_g}. \tag{3.77}$$

For $Z = 5$ this yields

$$p^{3D} = 5 \ a.u. \tag{3.78}$$

The corresponding momentum in 1D, for $Z = 5$, with a soft coulomb potential, was calculated to be

$$p^{1D} \approx 1.916 \ a.u. \tag{3.79}$$

The difference in momentum in a soft-coulomb potential compared to a proper-coulomb potential can explain the deviation in the ground state energy in 1D concerning what we would expect in 3D. However, none of these energy corrections affect the blue shift in energy we observe when we solve the time-dependent equations.

3.3 The time-dependent system

To evaluate how the system changes with time, we need to solve the time-dependent Schrödinger equation,

$$i\hbar\frac{\partial\left|\Psi\right\rangle}{\partial t} = H\left|\Psi\right\rangle. \tag{3.80}$$

We can express the wavefunction, $\Psi(x,t)$, as

$$|\Psi\rangle = \sum_n c_n(t)|\psi_n\rangle, \tag{3.81}$$

where $\psi_n(x)$ is the eigenvalue basis constructed in the previous section,

$$i\hbar\sum_n \dot{c}_n\left|\psi_n\right\rangle = \sum_n Hc_n\left|\psi_n\right\rangle, \tag{3.82}$$

where $\dot{c}_n = \frac{\partial c_n}{\partial t}$. Multiplying with $\langle\psi_m|$ from the left, we obtain the time-dependent matrix equation,

$$i\hbar\boldsymbol{S}\dot{\boldsymbol{c}}(t) = \boldsymbol{H}\boldsymbol{c}(t). \tag{3.83}$$

3.3.1 The Crank-Nicholson method

The electron initially starts in the ground state. To evaluate how the system changes with time, we need to construct a time propagator. This can be done by utilizing the Crank-Nicholson method[35]. The Crank-Nicholson method is a combination of the forward and backward Euler propagators [36]. The time propagator evaluates how the system changes with time step by step, where each step is expressed as Δt. The system's state is given by the vector elements in $\boldsymbol{c}(t)$, hence, we need to study how $\boldsymbol{c}(t)$ changes for each time step. By Taylor expanding $\boldsymbol{c}(t+\Delta t)$,

$$\boldsymbol{c}(t+\Delta t) \approx \boldsymbol{c}(t) + \dot{\boldsymbol{c}}(t)\Delta t, \tag{3.84}$$

we obtain an expression for $\dot{\boldsymbol{c}}(t)$,

$$\dot{\boldsymbol{c}}(t) \approx \frac{\boldsymbol{c}(t+\Delta t) - \boldsymbol{c}(t)}{\Delta t}. \tag{3.85}$$

This is known as the forward Euler propagator, and by inserting this into eq.(3.83), it yields

$$i\hbar\boldsymbol{S}\frac{\boldsymbol{c}(t+\Delta t) - \boldsymbol{c}(t)}{\Delta t} \approx \boldsymbol{H}\boldsymbol{c}(t). \tag{3.86}$$

Reorganizing this, eq.(3.86) becomes

$$\boldsymbol{c}(t+\Delta t) \approx \left(\mathbb{1} - \frac{i\Delta t}{\hbar}\boldsymbol{S}^{-1}\boldsymbol{H}\right)\boldsymbol{c}(t), \tag{3.87}$$

and, by letting $\Delta t \to \frac{\Delta t}{2}$, we obtain

$$\boldsymbol{c}\left(t+\frac{\Delta t}{2}\right) \approx \left(\mathbb{1} - \frac{i\Delta t}{2\hbar}\boldsymbol{S}^{-1}\boldsymbol{H}\right)\boldsymbol{c}(t). \tag{3.88}$$

As previously stated, the Crank-Nicholson method combines the forward and the backward Euler propagators. We obtain the backward Euler propagator by considering a backward time step in $\boldsymbol{c}(t)$. By Taylor expanding $\boldsymbol{c}(t-\Delta t)$,

$$\boldsymbol{c}(t-\Delta t) \approx \boldsymbol{c}(t) - \dot{\boldsymbol{c}}(t)\Delta t, \tag{3.89}$$

and reorganizing this equation, we obtain the backward Euler propagator,

$$\dot{\boldsymbol{c}}(t) \approx \frac{\boldsymbol{c}(t) - \boldsymbol{c}(t-\Delta t)}{\Delta t}. \tag{3.90}$$

As the forward Euler propagator, we insert this into eq.(3.83), and it yields

$$i\hbar \boldsymbol{S} \frac{\boldsymbol{c}(t) - \boldsymbol{c}(t-\Delta t)}{\Delta t} \approx \boldsymbol{H}\boldsymbol{c}(t). \tag{3.91}$$

By reorganizing this, eq.(3.91) becomes

$$\boldsymbol{c}(t-\Delta t) \approx \left(\mathbb{1} + \frac{i\Delta t}{\hbar}\boldsymbol{S}^{-1}\boldsymbol{H}\right)\boldsymbol{c}(t). \tag{3.92}$$

Now, by first letting $\Delta t \to \frac{\Delta t}{2}$, and then $t \to t + \Delta t$, we obtain the expression

$$\boldsymbol{c}\left(t + \frac{\Delta t}{2}\right) \approx \left(\mathbb{1} + \frac{i\Delta t}{2\hbar}\boldsymbol{S}^{-1}\boldsymbol{H}\right)\boldsymbol{c}(t+\Delta t), \tag{3.93}$$

which describes how the $\boldsymbol{c}$ changes for a time step $\frac{\Delta t}{2}$, as in eq.(3.88). By combining eq.(3.88) and eq.(3.93) we obtain the expression

$$\left(\boldsymbol{S} + \frac{i\Delta t}{2\hbar}\boldsymbol{H}\right)\boldsymbol{c}(t+\Delta t) = \left(\boldsymbol{S} - \frac{i\Delta t}{2\hbar}\boldsymbol{H}\right)\boldsymbol{c}(t), \tag{3.94}$$

where we define

$$\boldsymbol{M} = \boldsymbol{S} + \frac{i\Delta t}{2\hbar}\boldsymbol{H}. \tag{3.95}$$

By multiplying eq.(3.94) with $\boldsymbol{M}^{-1}$ from the left we obtain the Crank-Nicholson propagator

$$\boldsymbol{c}(t+\Delta t) = \boldsymbol{M}^{-1}\left(\boldsymbol{S} - \frac{i\Delta t}{2\hbar}\boldsymbol{H}\right)\boldsymbol{c}(t). \tag{3.96}$$

Due to the inversion of the $\boldsymbol{M}$ matrix, this propagator becomes very slow for larger matrices and requires a lot of computing power. However, it can be optimized using an algorithm based on the generalized minimal residual (GMRES) method as first proposed by Y. Saad and M. H. Schultz [37].

3.3.2 The GMRES method

The GMRES method is based on the Krylov subspace method and can solve linear systems, such as

$$\boldsymbol{A}\boldsymbol{x} = \boldsymbol{b}. \tag{3.97}$$

The Krylov subspace, denoted $\mathcal{K}_l$, is defined accordingly:

$$\mathcal{K}_l = \text{span}\{\boldsymbol{b}, \boldsymbol{Ab}, \ldots, \boldsymbol{A}^{l-1}\boldsymbol{x}\}. \tag{3.98}$$

Here the dimension of the $\boldsymbol{A}$ matrix is significantly greater than l. By using the Matlab script **lanczosprop.m**, which utilizes the Lanczos algorithm, we construct an orthogonal representation of the Krylov subspace [38],

$$\boldsymbol{A} = \boldsymbol{Q_l T_l Q_l}^T \tag{3.99}$$

where the columns in $\boldsymbol{Q_l}$ form the orthogonal basis of the Krylov subspace [39],

$$\boldsymbol{Q_l} = [\boldsymbol{q_1}, \boldsymbol{q_2}, \cdots, \boldsymbol{q_l}], \tag{3.100}$$

and the $\boldsymbol{T_l}$ is a $l \times l$ tridiagonal matrix.

An alternate is the Arnoldi algorithm to construct the orthogonal $\mathcal{K}_l$ basis,

$$\boldsymbol{AQ_l} = \boldsymbol{Q_{l+1}H_l}, \tag{3.101}$$

where $\boldsymbol{H_l}$ is an $(l+1) \times l$ upper Hessenberg matrix. The Arnoldi algorithm and Lanczos algorithm both construct orthogonal bases. The Arnoldi algorithm is applied when $\boldsymbol{A}$ is a non-hermitian matrix, and the Lanczos algorithm applies when the $\boldsymbol{A}$ matrix is hermitian [40]. By solving the small least square problem [39]

$$\boxed{\begin{gathered} \boldsymbol{x_l} = \boldsymbol{Q_l y_l} \\ \boldsymbol{y_l} \leftarrow \min ||\boldsymbol{T_l y_l} - \beta \boldsymbol{e_1}|| \\ \beta = ||\boldsymbol{b} - \boldsymbol{Ax_0}|| \end{gathered}} \tag{3.102}$$

where [40]

$$\boldsymbol{e_1} = \boldsymbol{Q_l} \frac{\boldsymbol{b} - \boldsymbol{Ax_0}}{||\boldsymbol{b} - \boldsymbol{Ax_0}||} \tag{3.103}$$

and $\boldsymbol{x_0}$ is an initial guess, we can approximate a solution for $\boldsymbol{x_l}$. Here $||\ldots||$ signifies the Euclidean norm. The Euclidean norm is defined as [40]

$$||\boldsymbol{x}|| = \sqrt{\boldsymbol{x} \cdot \boldsymbol{x}}. \tag{3.104}$$

We introduce a restart parameter by choosing l_{max} as an upper dimensional limit on the Krylov space, considering the GMRES being an iterative method. For $||\boldsymbol{b} - \boldsymbol{A}\boldsymbol{x}_{l_{max}}||$ greater than the accepted tolerance, the algorithm is restarted with $\boldsymbol{x_0} = \boldsymbol{x}_{l_{max}}$. This restart mechanism causes the GMRES method to be quite precise since the GMRES always minimizes the residual for each iteration step. However, for certain problems, the GMRES method has a particularly poor convergence rate. Hence, we modify the problem and apply the GMRES in the following system [39]:

$$\boldsymbol{M}^{-1}\boldsymbol{Ax} = \boldsymbol{M}^{-1}\boldsymbol{b}. \tag{3.105}$$

Applying this to the Crank-Nicholson propagator, we define

$$\boxed{\begin{aligned} \boldsymbol{A} &= \boldsymbol{S} + \tfrac{i\Delta t}{2\hbar}\boldsymbol{H} \\ \boldsymbol{b} &= \left(\boldsymbol{S} - \tfrac{i\Delta t}{2\hbar}\boldsymbol{H}\right)\boldsymbol{c}(t) \\ \boldsymbol{x} &= \boldsymbol{c}(t+\Delta t) \end{aligned}} \tag{3.106}$$

Ideally, we want to choose $\boldsymbol{M} = \boldsymbol{A}$ as in eq.(3.95) and eq.(3.96). However, this is not computationally feasible due to the inversion of the matrix, as previously discussed. Although it is sufficient to choose $\boldsymbol{M}$ matrix so that

$$\boldsymbol{M}^{-1}\boldsymbol{A} \approx \mathbb{1}. \tag{3.107}$$

Applying the $\boldsymbol{M}^{-1}$ matrix on the system substantially accelerates the convergence rate even though $\boldsymbol{M} \approx \boldsymbol{A}$. Thus we choose to express the $\boldsymbol{M}$ as [39]

$$\boldsymbol{M} = \boldsymbol{S} + \frac{i\Delta t}{2\hbar}\boldsymbol{H_0}, \tag{3.108}$$

where $\boldsymbol{H_0}$ is the time-independent Hamiltonian matrix constructed by the time-independent Hamiltonian. In eigenvalue basis, $\boldsymbol{S} = \mathbb{1}$ and $\boldsymbol{H_0} = \boldsymbol{D}$, which causes

$$\boxed{\begin{aligned} \boldsymbol{A} &= \mathbb{1} + \tfrac{i\Delta t}{2\hbar}\boldsymbol{D} + \boldsymbol{H_I} \\ \boldsymbol{b} &= \left(\mathbb{1} - \tfrac{i\Delta t}{2\hbar}\left(\boldsymbol{D} + \boldsymbol{H_I}\right)\right)\boldsymbol{c}(t) \\ \boldsymbol{x} &= \boldsymbol{c}(t+\Delta t) \\ \boldsymbol{M} &= \mathbb{1} + \tfrac{i\Delta t}{2\hbar}\boldsymbol{D}, \end{aligned}} \tag{3.109}$$

where $\boldsymbol{D}$ is the diagonal matrix containing the energy states of the system. This is due to the hermicity of the Hamiltonian operator. The eigenfunctions to different eigenvalues for a hermitian operator are orthogonal, as stated in section 2.1.1. This expression for $\boldsymbol{M}$ is a sparse matrix and saves a considerable amount of computing power. To save additional computing power, we utilize the incomplete lower-upper factorization on the $\boldsymbol{M}$ matrix for easier inversion [39].

Chapter 4

Results

As stated in the introduction, this thesis aims to study the shift in the energy spectra that occurs in the relativistic multi-photon ionization process. A super-intense X-ray laser pulse interacts with an electron in a hydrogen-like atom, and the resulting spectrum is compared with the non-relativistic equivalent. As seen in fig. 4.1 when the relativistic effects are considered, we observe a shift in the spectrum into higher energies, i.e., a relativistic blue shift, denoted as d in the inset in the figure. Each subsequent top in the figure represents one additional photon being absorbed by the electron [1]. It was recently found that the blue shift depended on the properties of the laser pulse, such as

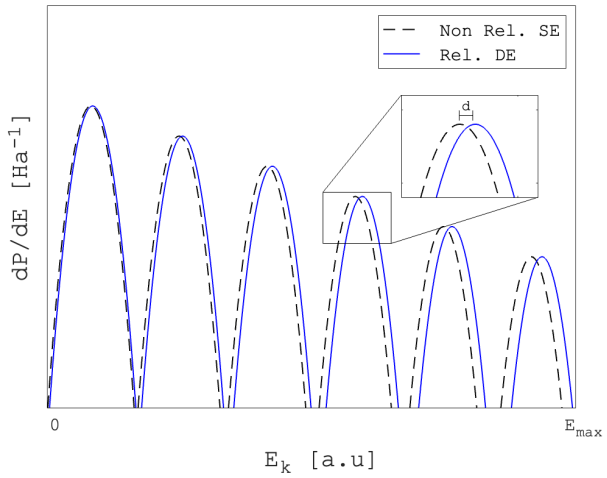

Figure 4.1: A model of the blue shift observed in the energy spectra under the multi-photon ionization process that occurs when a super intense X-ray laser pulse interacts with a hydrogen-like atom.

the radiation pressure and the laser's intensity, and it could be explained in terms of a temporal relativistic mass increase [2, 1]. Therefore, here, we propose that the blue shift may be caused by time dilation. To study this, we reduce the problem to a 1D system. We can think of this as if the electron is moving inside an extremely thin nanotube [16], within a narrow potential. The thin shape of the corresponding potential suggests that the electron's motion is restricted to 1D. This enables us to utilize the dipole approximation, which simplifies the problem significantly and allows us to study how the blue shift varies with the intensity of the laser.

4.1 The blue shift

To be able to study the blue shift, we need to simulate the multi-photon ionization process, as a super-intense X-ray laser pulse ionizes a hydrogen-like atom. This is done by solving for the time-dependent evolution of the system numerically, eq.(3.80), both within and beyond the nonrelativistic approximation.

The laser pulse is defined by the $\boldsymbol{A}$ potential and is given by

$$\boldsymbol{A}(t) = \begin{cases} \frac{E_0}{\omega} \sin^2\left(\frac{\pi t}{T_{pulse}}\right) \sin(\omega t)\hat{\boldsymbol{x}} & t \in [0, T_{pulse}] \\ 0 & t \notin [0, T_{pulse}] \end{cases} \tag{4.1}$$

where E_0 is the intensity, ω is the angular frequency, T_{pulse} is the duration of the laser pulse, and the unit vector $\hat{\boldsymbol{x}}$ defines the polarization direction. Here T_{pulse} can be expressed as $T_{pulse} = n\frac{2\pi}{\omega}$, where n is the number of periods of the laser pulse. The $\sin^2\left(\frac{\pi t}{T_{pulse}}\right)$ factor represent the pulse shape of the laser. Since we work in 1D, we can express the $\boldsymbol{A}(t)$ field potential as a scalar, i.e.,

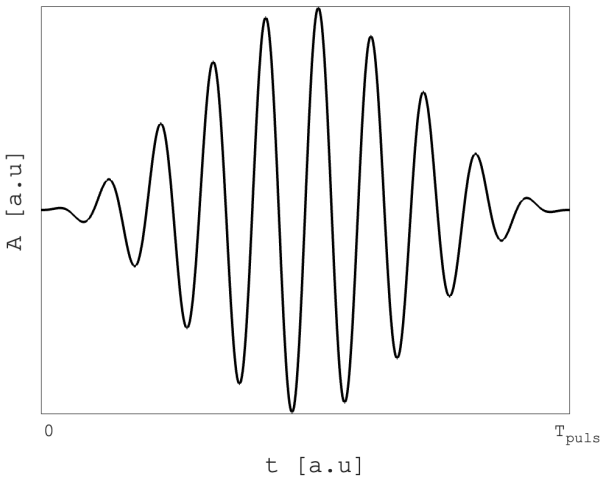

Figure 4.2: The laser pulse, with $T_{pulse} = 10\frac{\pi}{\omega}$.

$$\boldsymbol{A}(t) \to A_x(t) \equiv A(t), \tag{4.2}$$

$$A(t) = \frac{E_0}{\omega} \sin^2\left(\frac{\pi t}{T_{pulse}}\right) \sin(\omega t). \tag{4.3}$$

The pulse is shown in fig. 4.2.

We have simulated the multi-photon ionization process for $\omega = 50$ and $\omega = 80$ with varying intensities. To achieve a converged simulation for the highest intensity, we choose the following

parameters:

$$\begin{gathered} Z = 5 \\ E_0 = 1\,000 \text{ a.u.} \\ \omega = 50 \text{ a.u.} \\ N = 5\,000 \\ N_{dt} = 20\,000 \\ L = 85 \\ T_{pulse} = 10\frac{2\pi}{\omega} \text{ a.u.} \end{gathered} \tag{4.4}$$

Here T_{pulse} is the pulse duration, Z is the nuclear charge, N is the number of states, N_{dt} is the number of time steps, and L is the box size.

Following the multi-photon ionization process that has been simulated, both in non-relativistic and relativistic contexts, we then need to evaluate the probabilities of finding the electron in a specific energy state. This can be done by studying the energy spectra for the non-relativistic and relativistic processes. In the energy spectra, we evaluate the differential probability as a function of the electron's kinetic energy.

After the simulation, we are left with a vector $\boldsymbol{c}(T_{pulse})$, where the probability of finding the electron in each energy state n is given by

$$P_n(E_n) = |c_n(T_{pulse})|^2. \tag{4.5}$$

For energy levels $E_n \leq 0$, the electron is bound. Hence, by summing over the $|c_n(T_{pulse})|^2$ with the condition $E_n > 0$ we find the ionisation probability,

$$P_{ion} = \sum_{n=i}^{j} |c_n(T_{pulse})|^2, \tag{4.6}$$

where i and j is the first and last ionization state, respectively. Utilizing eq.(4.5) we can express the differential probability as

$$\frac{\mathrm{d}P}{\mathrm{d}E} = P_n(E_n)\rho(E_n), \tag{4.7}$$

where $\rho(E_n)$ is the density of states,

$$\rho(E_n) = \frac{2}{E_{n+1} - E_{n-1}}. \tag{4.8}$$

In fig. 4.3, we have plotted the energy spectra for the multi-photon ionization process. We have plotted the differential probability as a function of kinetic energy. In fig. 4.3a, we have plotted energy spectra for both the non-relativistic and relativistic systems with $E_0 = 1\,000$ a.u. and $\omega = 50$ a.u. For the non-relativistic system, we solved the TDSE, the black line, utilizing the Schrödinger Hamiltonian given in eq.(3.10). For the relativistic systems, we solved both the TDRSE, the blue line in the spectra, and the TDDE, the orange line, utilizing the relativistic Schrödinger Hamiltonian given in eq.(3.32) and the Dirac Hamiltonian given in eq.(3.15), respectively. Here each top, or group of tops, represents a photon-ionization or a photon being absorbed by the electron, also known as a photon resonance. As the electron absorbs photons, the order of the photon resonance increases, i.e., the first top in the energy spectra represents the probability of

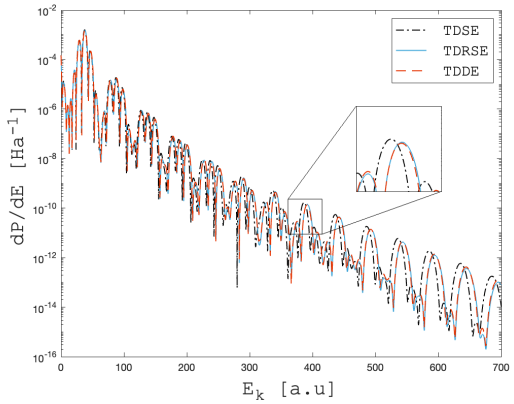

(a) $\omega = 50$ *and* $E_0 = 1000$

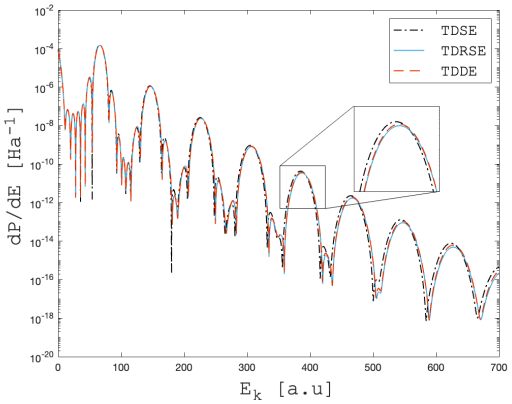

(b) $\omega = 80$ *and* $E_0 = 1000$

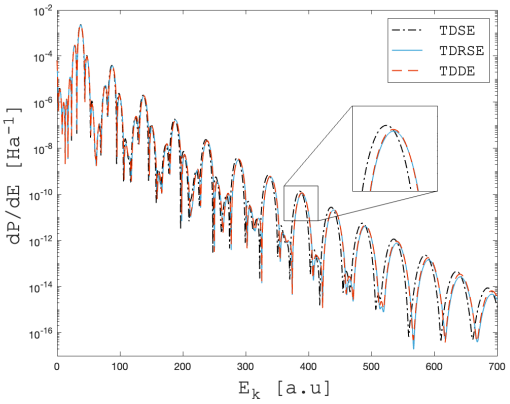

(c) $\omega = 50$ *and* $E_0 = 800$

Figure 4.3: The energy spectra for TDSE, TDRSE, and TDDE, with $N = 5000$*,* $N_{dt} = 20000$*,* $L = 85$*, and* $T_{pulse} = 10\frac{2\pi}{\omega}$*. The black line represents the non-relativistic TDSE, the blue line represents the TDRSE, and the orange line represents the TDDE. Here the zoomed-in section focuses on the photon resonance at approximately* $E_k \approx 400$ *a.u. For (a) and (c), this corresponds to photon resonance no. 8, and for (b), this corresponds to photon resonance no. 5.*

the electron having absorbed one photon, the second, two photons, and so on. In this figure, we see in total 13 photon resonances. For the lower-ordered photon resonances, there are a lot of oscillations, and instead of seeing a single well-defined photon resonance top, we have a group of tops. We also observe the relativistic blue shift in the kinetic energy as we compare the non-relativistic TDSE energy spectra to the relativistic TDRSE and TDDE. In the figure, we have zoomed in on photon resonance no. 8, which is the top near $E_k \approx 400$ a.u. Zooming in on this top, we observe that the TDRSE and TDDE energy spectra are virtually identical on the axis scale of the figure. In fig. 4.3b, we have plotted the same energy spectra as in fig. 4.3a, but with $\omega = 80$ a.u. Here we have zoomed in on photon resonance no. 5 as it is the closest top to $E_k \approx 400$ a.u. As in fig. 4.3a we observe the relativistic blue shift, however significantly smaller. In fig. 4.3c, we have plotted the same energy spectra, but with $E_0 = 800$ a.u. and $\omega = 50$ a.u. The zoomed-in section in this figure is at photon resonance top no. 5, as in fig. 4.3a. Here we observe a smaller shift than in fig. 4.3a but larger than in fig. 4.3b.

Comparing the relativistic blue shift for the photon resonance at about $E_k \approx 400$ a.u. we see that the blue shift both diminishes with decreasing intensity and with increasing angular frequency. This is consistent with the amplitude of the $A(t)$ field, given by $\frac{E_0}{\omega}$, which simply represents the

maximum velocity of a corresponding free electron moving in the laser field.

4.1.1 Dependency on the pulse duration

It is also interesting to study how the pulse duration affects the energy spectra. We do not expect that a prolonged pulse duration will have a significant effect on the relativistic blue shift. However, we expect it to affect the ionization probability.

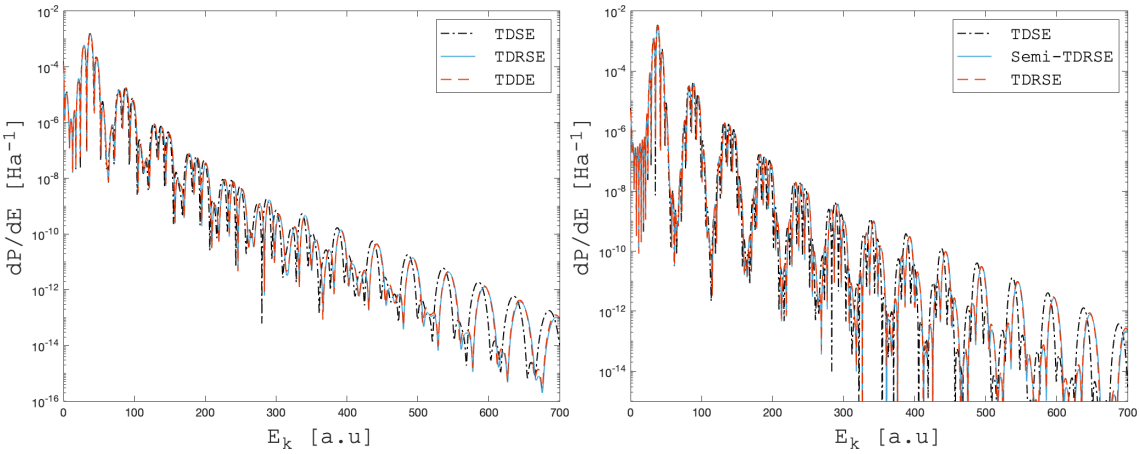

(a) $T_{pulse} = 10\frac{2\pi}{\omega}$ *(b)* $T_{pulse} = 15\frac{2\pi}{\omega}$

Figure 4.4: The energy spectra for TDSE, TDRSE, and TDDE, with $E_0 = 1000$, $\omega = 50$, $N = 5000$, $L = 85$, $N_{dt} = 20000$. *Here the black line represents the non-relativistic TDSE, the blue line represents the TDRSE, and the orange line represents the TDDE.*

In fig. 4.4, we have plotted the energy spectra for the multi-photon ionization process for the non-relativistic TDSE, the relativistic TDRSE, and the TDDE, and for a 10-cycle (left figure) and 15-cycle (right figure) laser pulse, respectively. In total, 13 photon resonances are depicted in the figures, and the relativistic blue shift is present in both cases. Comparing the energy spectra for the two pulses, we observe that the longer laser pulse causes more oscillations. The higher peaks in fig. 4.4b suggest a higher ionization probability, as shown in tab. 4.1, and is as expected.

	P_{ion}	
	$T_{pulse} = 10\frac{2\pi}{\omega}$	$T_{pulse} = 15\frac{2\pi}{\omega}$
TDSE	$1.19 \cdot 10^{-2}$	$1.74 \cdot 10^{-2}$
TDRSE	$1.17 \cdot 10^{-2}$	$1.71 \cdot 10^{-2}$
TDDE	$1.17 \cdot 10^{-2}$	$1.71 \cdot 10^{-2}$

Table 4.1: The ionization probability, P_{ion}, *of the multi-photon ionization process for a laser pulse with* 10 *and* 15 *periods.*

Evaluating how the pulse duration affects the blue shift, we measure the shift for the first four resonance tops in fig. 4.4a and fig. 4.4b, as shown in tab. 4.2. Due to the fast oscillations, the shift is calculated by choosing the middle of the resonance tops. The blue shift is calculated by measuring the separation of the non-relativistic and relativistic peak positions, respectively, for a given resonance. Considering some numerical uncertainties in the calculations of the shifts, we may conclude that the duration of the laser pulse does not affect the blue shift in a significant

way. Furthermore, the table shows that the shifts calculated with the TDRSE and TDDE are in agreement with each other.

	$T_{pulse} = 10\frac{2\pi}{\omega}$		$T_{pulse} = 15\frac{2\pi}{\omega}$	
no. Phot	d_{RSE}	d_{DE}	d_{RSE}	d_{DE}
1	0.37	0.37	0.37	0.37
2	0.93	0.92	0.92	0.91
3	1.53	1.49	1.54	1.51
4	2.20	2.12	2.22	2.16

Table 4.2: The blue shift observed in the energy spectra in fig. 4.4, for $T_{pulse} = 10\frac{2\pi}{\omega}$ and $T_{pulse} = 15\frac{2\pi}{\omega}$, with $E_0 = 1000$, $\omega = 50$, $N = 5000$, $L = 85$, $N_{dt} = 20000$. The blue shift observed for the TDDE is denoted d_{DE}, and for the TDRSE, it is denoted d_{RSE}.

4.1.2 Contribution of each correction term in the TDRSE

To get a better understanding of the relativistic blue shift, we now study how the role of each relativistic correction term in the TDRSE. In fig. 4.5, we have plotted the energy spectra for

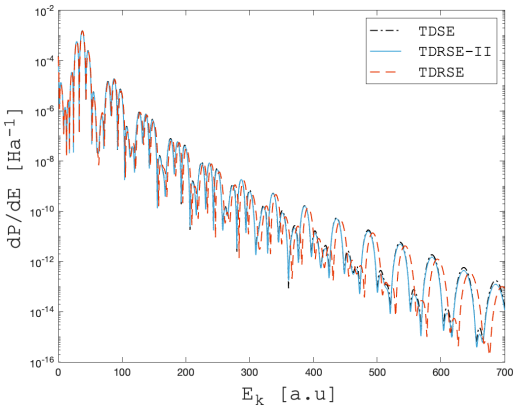

(a) TDRSE – II

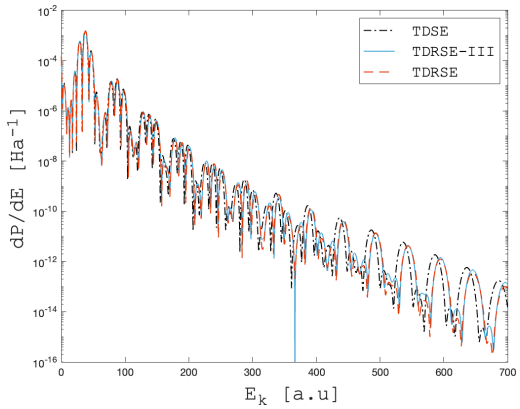

(b) TDRSE – III

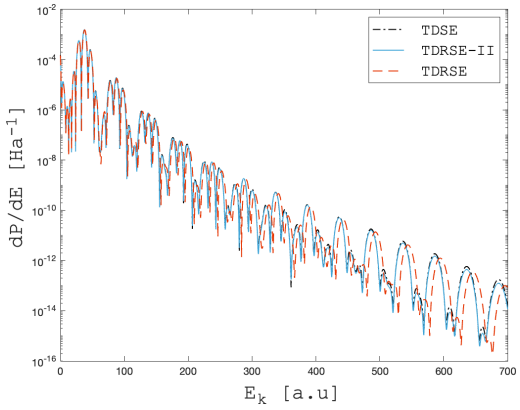

(c) TDRSE – IV

Figure 4.5: The energy spectra for the TDSE and TDRSE for each interaction term with $E_0 = 1000$, $\omega = 50$, $N = 2000$, $L = 65$, $N_{dt} = 5000$ and $T_{Pulse} = 10\frac{2\pi}{\omega}$. Here the black line represents the non-relativistic TDSE, and the blue line represents the TDRSE with the relevant interaction term. For fig. (a), we have plotted the energy spectra with interaction term II, in fig. (b), we have the interaction term III, and in (c), the interaction is term IV. The orange line represents the full TDRSE.

the multi-photon ionization process for the TDSE, TDRSE, and a modified TDRSE, which only contains one of the relativistic correction terms. The relativistic Schrödinger Hamiltonian is given by eq.(3.32),

$$H_{RSE} = \frac{p^2}{2m} + V - \underbrace{\frac{p^4}{8m^3c^2} + \frac{1}{8m^2c^2}\frac{\partial^2 V}{\partial x^2}}_{I} + \frac{e}{m}Ap - \underbrace{\frac{e}{2m^3c^2}A^3p}_{II} - \underbrace{\frac{3e^2}{4m^3c^2}A^2p^2}_{III} - \underbrace{\frac{e^3}{2m^3c^2}Ap^3}_{IV}, \quad (4.9)$$

where I is the relativistic structure correction term and II, III, and IV are the three transient relativistic correction terms. The figures 4.5 (a-c) show the energy spectra for the modified TDRSE with the correction terms II, III, and IV, denoted TDRSE-II, TDRSE-III, and TDRSE-IV, respectively. In the figures, we observe that the energy spectra for the TDRSE-II and TDRSE-IV are essentially on top of the energy spectra for the non-relativistic TDSE. Therefore we can conclude that the terms II and IV do not contribute significantly to the relativistic blue shift. However, the energy spectrum for the TDRSE-III is on top of the energy spectra for the TDRSE. Hence, we can conclude that term III contributes to the blue shift and is the most prominent of the transient interaction terms in eq.(4.9).

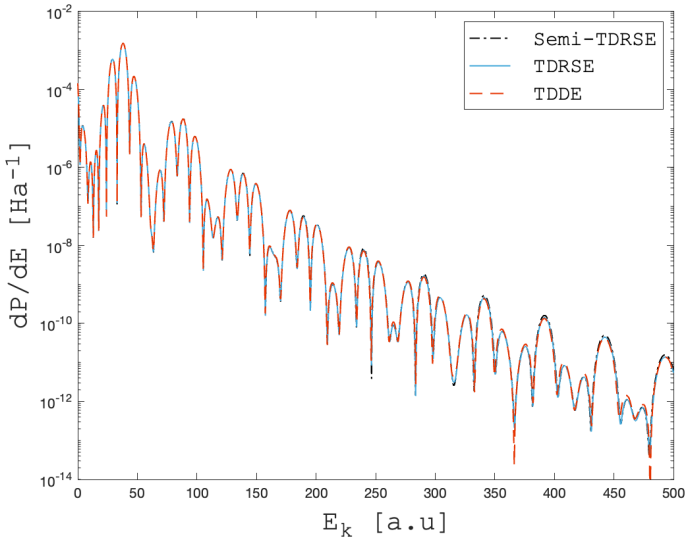

Figure 4.6: The energy spectra for the TDRSE, TDDE, and the semi-TDRSE, where we omit the term I form the relativistic Schrödinger Hamiltonian, with $E_0 = 1000$, $\omega = 50$, $N = 1\,500$, $L = 65$, $N_{dt} = 10\,000$ *and* $T_{Pulse} = 10\frac{2\pi}{\omega}$.

In fig. 4.6, we have plotted the energy spectra for the multi-photon ionization process for the TDRSE, TDDE, and a modified TDRSE, denoted semi-TDRSE, where we omit the relativistic structure effects in term I. We observe that all the energy spectra in the figure are essentially identical. The only divergence is that the peaks of the energy spectrum for the semi-TDRSE are slightly higher for the higher-order photon resonances. However, the peak position does not seem to be affected. We may therefore conclude that the relativistic structure effects are of minor importance in the multi-photon ionization process.

4.2 Multi photon ionization described by time dilation

The blue shift appears to vary with the intensity, E_0, and angular frequency, ω, of the laser pulse. By studying the energy spectra in fig. 4.3, we observe that for each photon-ionization, the shift in energy increases. The electron apparently absorbs a more energetic photon for each photon resonance top, with respect to the non-relativistic results. As just stated, the term causing the relativistic blue shift is derived from the relativistic mass correction. However, here we propose that the behavior of the blue shift can be described and modeled by the relativistic effect of time dilation.

4.2.1 Time dilation

According to special relativity, time is relative, and the faster we move through space, the slower we move through time. This is what's known as time dilation and was introduced in section 2.2.1. As previously stated, the theory of special relativity describes how time, length, and mass behave in an accelerated reference frame compared to an internal one. The time dilation, as given in eq.(2.41),

$$\Delta t = \gamma \Delta t', \tag{4.10}$$

where $\Delta t'$ is the proper time, i.e., the time measured in the accelerated frame. This equation describes how the time in an accelerated reference frame relates to the time measured by an observer in an inertial rest frame [18]. Here the primed system is the accelerated frame, and the unprimed system is the rest frame. One of the postulates of special relativity states that the speed of light in a vacuum is the same for all inertial reference frames and is not affected by the movement of the source, denoted as c. Utilizing this, we manipulate eq.(4.10), and acquire a relation for the angular frequency experienced in the rest frame, ω, and the angular frequency experienced in the accelerated frame, ω':

$$\begin{array}{|c|} \hline \Delta t = \gamma \Delta t' \\ \\ \frac{1}{\Delta t} = \frac{1}{\gamma \Delta t'} \\ \\ \gamma f = f' \\ \\ \gamma 2\pi\omega = 2\pi\omega' \\ \\ \gamma\omega = \omega' \\ \hline \end{array} \quad \Rightarrow \quad \begin{array}{|c|} \hline \Delta t > \Delta t' \\ \\ \frac{1}{\Delta t} < \frac{1}{\Delta t'} \\ \\ f < f' \\ \\ 2\pi\omega < 2\pi\omega' \\ \\ \omega < \omega' \\ \hline \end{array} \tag{4.11}$$

The last line in this derivation yields the relation $\gamma\omega = \omega'$, which causes $\omega < \omega'$. Utilizing the angular frequency's relation to energy,

$$E = \hbar\omega, \tag{4.12}$$

we expect the energy of the photons on the accelerated frame to be more energetic than in a rest frame. This is what we observe in the energy spectra. By considering the non-relativistic Schrödinger equation as the unprimed system and the relativistic equations as the primed system, we can evaluate the time dilation experienced by the electron at each photo-ionization. Utilizing this, we can construct a model that predicts and describes how the blue shift behaves.

4.2.2 Lorentz factor in the velocity gauge

When we solved the time-dependent equations, we solved them in the velocity gauge. In the velocity gauge, and considering a super intense laser field, the majority of the momentum is carried by the vector potential A, and the proper momentum, p, can be considered constant throughout the interaction. Utilizing minimal coupling, we can therefore express the Lorentz factor as

$$\gamma = \sqrt{1 + \left(\frac{p}{mc}\right)^2} \quad \Rightarrow \quad \gamma = \sqrt{1 + \left(\frac{p + eA}{mc}\right)^2} \tag{4.13}$$

in the velocity gauge. As discussed in section 3.2.4, the momentum in the ground state in a soft-Coulomb potential is significantly smaller than for a proper-Coulomb potential. The initial momentum in the non-relativistic system was calculated to be $p \approx 1.916$ a.u.

4.2.3 The semi-quantized field

For each photo-ionization, a photon is annihilated and absorbed by the electron. A classical A field is not sufficient to describe this annihilation process because it cannot describe the behavior of the individual photons. Hence, we need to introduce a quantized photon field A_q. However, utilizing a purely quantized photon field is also unsuitable due to the intensity of the laser pulse. Therefore we propose a semi-quantized approach.

By choosing to keep the classical photon field as in eq.(4.3),

$$A_{cl}(t) = \frac{E_0}{\omega} \sin^2\left(\frac{\pi t}{T_{pulse}}\right) \sin(\omega t), \tag{4.14}$$

we construct the semi-quantized photon field, henceforth denoted A, as

$$A(t) = A_{cl}(t) - A_q(t), \tag{4.15}$$

where A_q is the quantized photon field. The number state of the A_q field only contains the necessary number of photons to be annihilated for the relevant photon resonance top. We subtract A_q from A_{cl} to mimic the absorption process of the photon, effectively causing the modified field becomming weaker. The quantized photon field, A_q, is constructed as in section 2.3.4. By making some assumptions, i.e., that we have monochromatic light, horizontal polarization, $\hat{\varepsilon} = 1$, that there is no emission/creation of photons and reducing the system to 1D (utilizing the dipole approximation), the quantized photon field becomes

$$A_q(t) = -i\frac{E_0}{\omega}\hat{a}e^{-i\omega t}. \tag{4.16}$$

The semi-quantized photon field then takes the form

$$A = \frac{E_0}{\omega} \sin^2\left(\frac{\pi t}{T_{puls}}\right) \sin(\omega t) + i\frac{E_0}{\omega}\hat{a}e^{-i\omega t}. \tag{4.17}$$

4.2.4 Modeling multiphoton ionization

Utilizing the Lorentz factor expressed with $p \to p + eA$, eq.(4.13), the semi-quantized A field that describes the annihilation process, eq.(4.17), and the relation for the angular frequency experienced in an accelerated frame compared to in an inertial rest frame, eq.(4.11), we can construct a simple model that describes the multi-photon ionization process. We need to evaluate the time dilation experienced by the electron after each photon-ionization and update the A field with the experienced angular frequency, ω. For n'th photon resonance, the A_q acts on a photon number state $|n\rangle$, and we can express the model as

$$\begin{array}{lll} A_0 = A_{cl}(\omega_0) + i\frac{E_0}{\omega_0}e^{-i\omega_0 t}\sqrt{n} & \gamma_0 = \sqrt{1 + \left(\frac{p+eA_0}{mc}\right)^2} & \omega_1 = |\gamma_0\omega_0| \\ A_1 = A_{cl}(\omega_1) + i\frac{E_0}{\omega_1}e^{-i\omega_1 t}\sqrt{n-1} & \gamma_1 = \sqrt{1 + \left(\frac{p+eA_1}{mc}\right)^2} & \omega_2 = |\gamma_1\omega_1| \\ \vdots & \vdots & \vdots \\ A_{n-1} = A_{cl}(\omega_{n-1}) + i\frac{E_0}{\omega_{n-1}}e^{-i\omega_{n-1} t}\sqrt{1} & \gamma_{n-1} = \sqrt{1 + \left(\frac{p+eA_{n-1}}{mc}\right)^2} & \omega_n = |\gamma_{n-1}\omega_{n-1}| \end{array} \tag{4.18}$$

We take the absolute value of the ω because the ω_n has an imaginary part. The imaginary part is relatively small and does not significantly impact the results. It is also worth noting that since the number state of the A_q field exactly contains the necessary number of photons for each photon resonance, the ω_4 in the 4th step in the sixth order photon resonance is NOT the same ω_4 as in the fourth order photon resonance.

4.2.5 Results of modeling the blue shift in 1D

As previously stated, the relativistic blue shift is dependent on the amplitude, $\frac{E_0}{\omega}$, of the vector potential. Utilizing the model described in eq.(4.18) we can predict how the blue shifts evolve with intensity. To evaluate if our model can accurately describe the relativistic blue shift, we study the shift in the multi-photon ionization process with different angular frequencies and intensities.

In fig. 4.7 (a-f), we have plotted the energy spectra for the non-relativistic TDSE, the relativistic TDRSE, and the TDDE, for intensities, $E_0 = 1\,000$ (left panels), $E_0 = 800$ (middle panels) and $E_0 = 600$ a.u. (right panels). The upper and lower panels show the results for $\omega = 50$ and $\omega = 80$ a.u., respectively. We observe that the shift diminishes with decreasing laser intensities for both frequencies. Moreover, again there is good agreement between the TDRSE and TDDE results.

As before, in order to calculate the relativistic blue shift, we measure the shift between the peaks of the non-relativistic and relativistic in the energy spectra for the given photon resonance. In tab. 4.3 and tab. 4.4, we have studied the blue shift for $\omega = 50$ and $\omega = 80$ a.u., respectively. In both cases we have chosen the intensities $E_0 = 1\,000$ and $E_0 = 600$ a.u. The tables gives the predicted angular frequency of the photon, ω, at each photon resonance and the expected blue

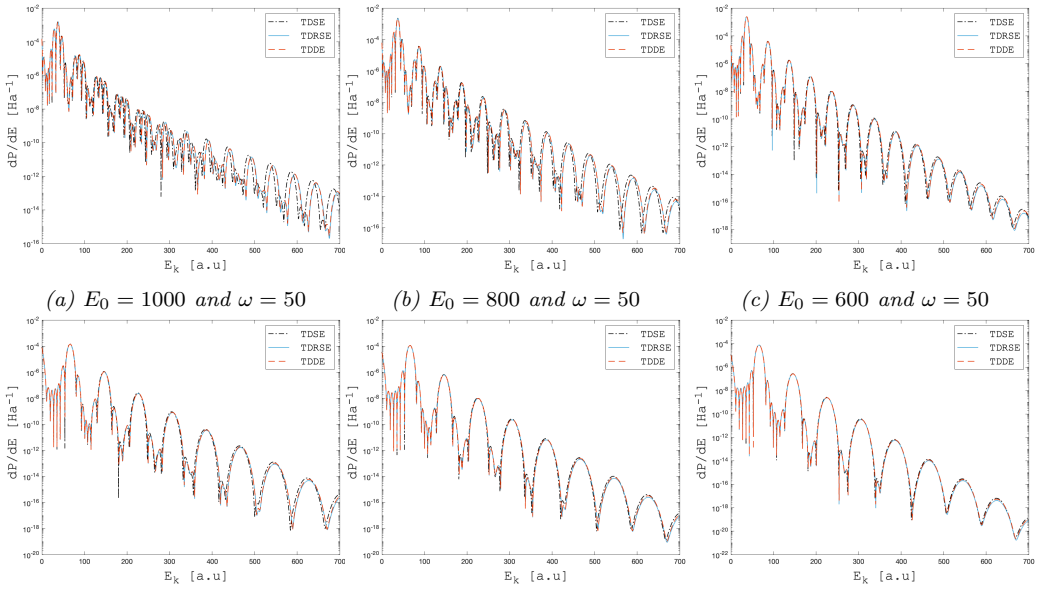

(a) $E_0 = 1000$ *and* $\omega = 50$ *(b)* $E_0 = 800$ *and* $\omega = 50$ *(c)* $E_0 = 600$ *and* $\omega = 50$

(d) $E_0 = 1000$ *and* $\omega = 80$ *(e)* $E_0 = 800$ *and* $\omega = 80$ *(f)* $E_0 = 600$ *and* $\omega = 80$

Figure 4.7: The energy spectra for TDSE, TDRSE, and TDDE, with $N = 5000$, $N_{dt} = 20000$, $T_{pulse} = 10\frac{2\pi}{\omega}$, $L = 85$. *With varying intensity and angular frequency. The black line represents the TDSE, the blue line is the TDRSE, and the orange line is the TDDE.*

shift d. The observed relativistic blue shift in the results for the TDDE and TDRSE is denoted d_{DE} and d_{RSE}, respectively.

$E_0 = 1000$ and $\omega = 50$					$E_0 = 600$ and $\omega = 50$				
	Predicted		Observed			Predicted		Observed	
no. Phot	ω	d	d_{RSE}	d_{DE}	no. Phot	ω	d	d_{RSE}	d_{DE}
1	50.37	0.37	0.37	0.37	1	50.14	0.14	0.14	0.14
2	50.84	0.84	0.93	0.92	2	50.31	0.31	0.36	0.36
3	51.38	1.38	1.53	1.49	3	50.51	0.51	0.61	0.60
4	52.00	2.00	2.20	2.12	4	50.74	0.74	0.87	0.85
5	52.67	2.67	2.89	2.78	5	50.96	0.96	1.13	1.10
6	53.39	3.39	3.61	3.46	6	51.25	1.25	1.41	1.37
7	54.13	4.13	4.40	4.20	7	51.54	1.54	1.69	1.63
8	54.92	4.92	5.19	4.92	8	51.84	1.84	1.98	1.90
9	55.73	5.73	6.01	5.70	9	52.16	2.16	2.25	2.16
10	56.57	6.57	6.84	6.44	10	52.50	2.50	2.54	2.44

Table 4.3: The blue shift for $\omega = 50$ *with* $E_0 = 1\,000$ *a.u. and* $E_0 = 600$ *a.u. as predicted by our model, eq.(4.18), and observed in 4.7. The predicted angular frequency experienced by the relativistic electron is denoted* ω, *and the predicted blue shift is denoted* d. *The observed shift for the TDRSE is denoted* d_{RSe} *and* d_{DE} *for the TDDE.*

Comparing the blue shift for the TDRSE to the TDDE, we observe that the shifts are quite similar for lower-ordered photon resonances. However, for the results with higher intensities, the blue shift for the TDRSE and TDDE tends to diverge for the higher-ordered photon resonances, merely reflecting the fact in the limit of very high energies, the semi-relativistic approximation ultimately breaks down. This is due to the approximation we do when constructing the relativistic

Schrödinger Hamiltonian, where we omit the correction terms of order $\mathcal{O}\left(\frac{1}{c^3}\right)$ and higher, especially the p^6 correction term, which will produce more temporal interaction terms.

$E_0 = 1000$ and $\omega = 80$					$E_0 = 600$ and $\omega = 80$				
	Predicted		Observed			Predicted		Observed	
no. Phot	ω	d	d_{RSE}	d_{DE}	no. Phot	ω	d	d_{RSE}	d_{DE}
1	80.24	0.24	0.28	0.27	1	80.09	0.09	0.10	0.10
2	80.54	0.54	0.67	0.67	2	80.21	0.21	0.23	0.23
3	80.90	0.90	1.10	1.07	3	80.34	0.34	0.39	0.39
4	81.28	1.28	1.55	1.51	4	80.49	0.49	0.54	0.54
5	81.71	1.71	2.02	1.94	5	80.65	0.65	0.70	0.70
6	82.17	2.17	2.51	2.40	6	80.82	0.82	0.86	0.86
7	82.66	2.66	2.98	2.83	7	81.00	1.00	1.02	0.95
8	83.19	3.19	3.47	3.30	8	81.19	1.19	1.18	1.26

Table 4.4: The blue shift for $\omega = 80$ with $E_0 = 1\,000$ a.u. and $E_0 = 600$ a.u. as predicted by our model, eq.(4.18), and observed in 4.7. The predicted angular frequency experienced by the relativistic electron is denoted ω, and the predicted blue shift is denoted d. The observed shift for the TDRSE is denoted d_{RSe} and d_{DE} for the TDDE.

Comparing the blue shift for the TDDE to the shift predicted by eq.(4.18), we observe that there is a good agreement between our predictions and what is observed in the TDDE. However, for the lower-ordered photo resonances, the predicted shift generally seems to be a bit too low, and for the higher-ordered photon resonances, it appears to be a bit too high. The deviations between the modeled d and the d_{DE} the lower-ordered photo resonances are at a maximum of 20% of the d_{DE}. The general trend is that the error decreases with increasing order of the photon resonances. The deviations between our model and the result in the TDDE may be caused by the approximations and assumptions we made when constructing our model.

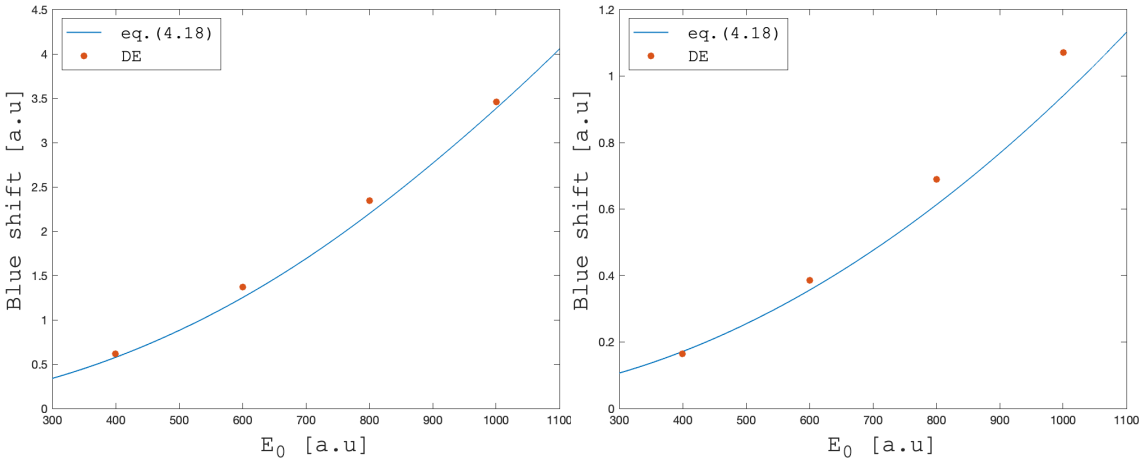

(a) $\omega = 50$ Phot. no. 6 *(b) $\omega = 80$ Phot. no. 3*

Figure 4.8: Blue shift as a function of E_0 for photon ionization resonance no. 6 for $\omega = 50$ and photon ionization resonance no. 3 for $\omega = 80$. The blue linen is predicted by eq.(4.18), and the red dots are the blue shift observed in the results of the TDDE.

Finally, we would like to evaluate how the intensity of the laser pulse affects the blue shift for a specific photon resonance. In fig. 4.8 (a-b), we have potted the blue shift predicted from eq.(4.18),

in blue as a function of the intensity for the given photon resonance. In fig. 4.8a (left), we have chosen $\omega = 50$ and photon resonance no. 6, and in fig. 4.8b (right), we have chosen $\omega = 80$ a.u., and photon resonance no. 3. The red dots in both figures are the blue shift observed for the TDDE. Here we observe a good agreement between our prediction and the blue shift in the results for the TDDE. The relative error in fig. 4.8b is somewhat larger, but this is merely due to the shift for lower-ordered photon resonances being quite small and, therefore, the error for our model becomes high in comparison.

Chapter 5

Conclusion and outlook

In summary, this thesis has studied the relativistic multi-photon ionization process as a super-intense X-ray laser pulse ionizes a hydrogen-like atom. By restricting the movement of the ionized electron to 1D, we have studied this multi-photon ionization process in both relativistic and non-relativistic contexts. It was found that the kinetic energy of the emitted photo-electron is higher in the relativistic limit, i.e., a relativistic blue shift is observed in the corresponding energy spectra. By utilizing time dilation, we were able to model and describe the underlying processes involved in the relativistic light-matter interaction.

We studied the multi-photon ionization process by utilizing Matlab to solve the time-dependent Dirac and Schrödinger equations. We also constructed a relativistic Schrödinger equation by utilizing the Foldy-Wouthuysen transformation on the Dirac Hamiltonian [17], to be able to single out the type of interaction that is causing the relativistic blue shift. As it turns out, the results of the numerical calculation with the time-dependent Dirac (TDDE) and the relativistic Schrödinger (TDRSE) equations are in good agreement. Nonetheless, they tend to diverge for very laser intensities and at higher-ordered photon resonances. This merely demonstrates that the semi-relativistic approach ultimately breaks down when approaching the ultra-relativistic limit. By inspecting the role of the different terms in the relativistic Schrödinger Hamiltonian on ionization dynamics, we were able to identify which relativistic corrections contribute the most to the relativistic blue shift. We found that the blue shift was caused by a temporal relativistic effect, which can be attributed to a transient relativistic mass increase. As such, we found that the relativistic structure corrections had no significant effect on the blue shift.

As the relativistic electron is oscillating in the intense laser field, it undergoes time dilation due to its relativistic speeds. Which then causes the corresponding increases in the experienced laser frequency, i.e., a blue shift. By varying the laser's intensity, E_0, and angular frequency, ω, we concluded that the relativistic blue shift increases with increasing intensity and decreasing angular frequency. This is consistent with the amplitude of the vector potential, given by $\frac{E_0}{\omega}$, which represents the maximum velocity of a corresponding free electron moving in the laser field. We also found that the laser pulse duration does not affect the blue shift.

Even though the relativistic correction term causing the blue shift is derived from the relativistic mass increase, it is easier to explain the relativistic multi-photon ionization process utilizing time dilation. As the super-intense laser pulse ionizes the electron, it may absorb multiple photons in succession. For each subsequent photon-ionization, it appears as the electron absorbs a more energetic photon compared to the non-relativistic equivalent. Utilizing a semi-quantized field

approach, we constructed the laser field experienced by the relativistic electron at each photon resonance in comparison to the field experienced by its corresponding non-relativistic counterpart. The difference in the frequency of the photons experienced by the relativistic electron, with respect to the corresponding non-relativistic one, determines the blue shift.

In this work, we have studied the blue shift in 1D. However, to be able to conclude that the relativistic blue shift really exists, we need to study a 3D system. Reducing the system to 1D simplified the problem significantly and allowed us to identify some of the mechanisms involved in the relativistic multi-photon ionization process. In 3D, on the other hand, we also need to consider the beyond dipole effects that occur when we keep the space dependency in the vector potential. It has recently been shown that the non-dipole effects may lead to a corresponding red-shifting of energy spectra [1, 2]. Implementing the beyond dipole effects can be challenging in terms of the Dirac equation, and it is, therefore, advantageous to make some approximations, like utilizing a Taylor expansion of the vector potential. To be able to utilize the Taylor expansion successfully, the Dirac Hamiltonian needs to be modified [41]. A modified Dirac Hamiltonian, which allows for Taylor expansion of the vector potential, is derived in appendix B and will be tested and utilized by the research group to study the multi-photon ionization process in 3D, and it has already produced promising results (not shown here) [34].

Appendix A

Foldy-Wouthuysen transformation

When utilizing the FW transformation [17] on the Dirac Hamiltonian, using the Baker-Campbell Hausdorff formula, eq.(2.64), we need to calculate each correction term arising from the commutation relations. The calculation of these correction terms for this transformation differs in 3D and 1D. The details of these calculations are outlined in this appendix.

A.1 3D FW transformation

Dirac Hamiltonian is defined by

$$H_{DE} = c\boldsymbol{\alpha} \cdot (\boldsymbol{p} + e\boldsymbol{A}) + \mathbb{1}V + \beta mc^2. \tag{A.1}$$

Defining the operators as

$$o = c\boldsymbol{\alpha} \cdot (\boldsymbol{p} + e\boldsymbol{A}) \quad \text{and} \quad \varepsilon = \mathbb{1}V, \tag{A.2}$$

where o and ε are odd and even operators, respectively. The transformation is given by

$$S = -\frac{i\beta o}{2mc^2}. \tag{A.3}$$

The transformed Hamiltonian is given by [17]

$$H'_{DE} = \beta\left(mc^2 + \frac{o^2}{2mc^2} - \frac{o^4}{8m^3c^6}\right) - \frac{1}{8m^2c^4}[o,[o,\varepsilon] + i\dot{o}]. \tag{A.4}$$

Calculating each of the terms, we begin with

$$o^2 = c^2(\boldsymbol{p} + e\boldsymbol{A})^2 + c^2 e\boldsymbol{\sigma}_{4\times4} \cdot \boldsymbol{B}. \tag{A.5}$$

Here we used the fact the $\boldsymbol{\alpha}$ is constructed using Pauli matrices that follow this relation [17]:

$$\boldsymbol{\sigma} \cdot \boldsymbol{a}\, \boldsymbol{\sigma} \cdot \boldsymbol{b} = \boldsymbol{a} \cdot \boldsymbol{b} + i\boldsymbol{\sigma} \cdot \boldsymbol{a} \times \boldsymbol{b} \tag{A.6}$$

Next

$$o^4 = c^4(\boldsymbol{p} + e\boldsymbol{A})^4, \tag{A.7}$$

Here the terms containing $\boldsymbol{B}$ have been omitted. This is due to $\boldsymbol{B}$ being of order $\mathcal{O}\left(\frac{1}{c}\right)$, which causes these terms to be of $\mathcal{O}\left(\frac{1}{c^3}\right)$. Now by expressing

$$\boldsymbol{E} = -\nabla\phi - \frac{\partial \boldsymbol{A}}{\partial t}, \tag{A.8}$$

we obtain

$$[o, \varepsilon] + i\dot{o} = -cei\boldsymbol{\alpha} \cdot \boldsymbol{E}, \tag{A.9}$$

and

$$[o, [o, \varepsilon] + i\dot{o}] = -c^2 e(\nabla \cdot \boldsymbol{E} + 2\boldsymbol{\sigma}_{4\times4} \cdot \boldsymbol{E} \times (\boldsymbol{p} + e\boldsymbol{A}) + i\boldsymbol{\sigma}_{4\times4} \cdot \nabla \times \boldsymbol{E}). \tag{A.10}$$

The H'_{DE} then becomes

$$\begin{aligned} H'_{DE} = \beta\left(mc^2 + \frac{(\boldsymbol{p}+e\boldsymbol{A})^2}{2m} - \frac{(\boldsymbol{p}+e\boldsymbol{A})^4}{8m^3c^2}\right) + \mathbb{1}V + \frac{e}{2m}\boldsymbol{\sigma}_{4\times4} \cdot \boldsymbol{B} \\ + \mathbb{1}\frac{e}{8m^2c^2}\nabla \cdot \boldsymbol{E} + \mathbb{1}\frac{e}{4m^2c^2}\boldsymbol{\sigma}_{4\times4} \cdot \boldsymbol{E} \times \boldsymbol{p} + \mathbb{1}\frac{ie}{8m^2c^2}\boldsymbol{\sigma}_{4\times4} \cdot \nabla \times \boldsymbol{E} \end{aligned} \tag{A.11}$$

A.2 1D FW transformation

Starting with the 1D Dirac Hamiltonian,

$$H_{DE} = c\alpha(p + eA) + \mathbb{1}V + \beta mc^2. \tag{A.12}$$

Defining the operators as

$$o = c\alpha(p + eA) \quad \text{and} \quad \varepsilon = \mathbb{1}V, \tag{A.13}$$

where o and are odd and even operators, respectively. The transformation is given by

$$S = -\frac{i\beta o}{2mc^2}. \tag{A.14}$$

The transformed Hamiltonian is given by [17]

$$H'_{DE} = \beta\left(mc^2 + \frac{o^2}{2mc^2} - \frac{o^4}{8m^3c^6}\right) - \frac{1}{8m^2c^4}[o, [o, \varepsilon] + i\dot{o}]. \tag{A.15}$$

The terms are given by:

$$o^2 = c^2(p + eA)^2, \tag{A.16}$$

$$o^4 = c^4(p + eA)^4. \tag{A.17}$$

By utilizing

$$E = -\frac{\partial\phi}{\partial x} - \frac{\partial A}{\partial t}, \tag{A.18}$$

we obtain

$$[o, \varepsilon] + i\dot{o} = -cei\alpha E, \tag{A.19}$$

$$[o, [o, \varepsilon] + i\dot{o}] = -c^2 e\frac{\partial E}{\partial x} = -c^2\frac{\partial^2 V}{\partial x^2}. \tag{A.20}$$

The H'_{DE} then becomes

$$\begin{aligned} H'_{DE} = \beta \left(mc^2 + \frac{(p+eA)^2}{2m} - \frac{(p+eA)^4}{8m^3c^2} \right) + \mathbb{1}V \\ + \mathbb{1}\frac{1}{8m^2c^2}\frac{\partial^2 V}{\partial x^2} \end{aligned} \tag{A.21}$$

Appendix B

3D beyond dipole Dirac Hamiltonian

As stated in the conclusion, it can be challenging to implement the beyond-dipole effects when studying a relativistic system. It may therefore be advantageous to utilize a Taylor expansion for the vector potential. However, it has proven challenging to implement a Taylor expanded $\boldsymbol{A}(\boldsymbol{x}, t)$ in the Dirac equation [41]. The problem arises due to the $\boldsymbol{A}^2(\boldsymbol{x}, t)$ implicitly being present in the Dirac Hamiltonian. This becomes evident when we do the FW transformation on the Dirac Hamiltonian. The Taylor expanded vector potential is given by

$$\boldsymbol{A}(x,t) = \boldsymbol{A_0}(t) + \frac{x}{c}\boldsymbol{E_0}(t) - \frac{x^2}{2c^2}\dot{\boldsymbol{E}}_{\boldsymbol{0}} + \dots \tag{B.1}$$

and the vector potential squared is given by

$$\boldsymbol{A}^2(x,t) = \boldsymbol{A_0}^2(t) + 2\frac{x}{c}\boldsymbol{A_0}\boldsymbol{E_0}(t) + \frac{x^2}{c^2}\boldsymbol{E_0}^2 - \frac{x^2}{c^2}\boldsymbol{A_0}\dot{\boldsymbol{E}}_{\boldsymbol{0}} + \dots \tag{B.2}$$

If we truncate eq.(B.1) to only contain terms of $\mathcal{O}\big(\frac{1}{c}\big)$ and lower, the $\boldsymbol{A}^2(x,t)$ becomes

$$\boldsymbol{A}^2(x,t) \approx \boldsymbol{A_0}^2(t) + 2\frac{x}{c}\boldsymbol{A_0}\boldsymbol{E_0}(t) + \frac{x^2}{c^2}\boldsymbol{E_0}^2. \tag{B.3}$$

Here we see that even if we truncate the $\boldsymbol{A}(x,t)$ potential the $\boldsymbol{A}^2(x,t)$ still contains a term of order $\mathcal{O}\big(\frac{1}{c^2}\big)$. Furthermore, it only contains half of the $\mathcal{O}\big(\frac{1}{c^2}\big)$ contribution in eq.(B.2). As it turns out, the effect of the two terms are of similar magnitude but of opposite signs [41, 25]. When only one of them is included, as is effectively the case of the Dirac Hamiltonian with a Taylor expanded vector potential, it causes a significant error in the time-dependent evolution of the simulation, producing poor results. Since $\boldsymbol{A}^2(x,t)$ is only implicitly present in the Dirac Hamiltonian, we can not easily exclude the higher-ordered terms from the $\boldsymbol{A}^2(x,t)$ potential. Hence, it is advantageous to modify the Dirac Hamiltonian so that we have an expression where the $\boldsymbol{A}^2(x,t)$ is explicitly present.

B.1 Dipole approximation w/ beyond dipole correction terms

The Dirac equation is given by,

$$i\hbar\frac{\partial\psi}{\partial t} = H\psi, \tag{B.4}$$

where

$$H = c\boldsymbol{\alpha}\cdot(\boldsymbol{p} + e\boldsymbol{A}) + \beta mc^2 + \mathbb{1}V, \tag{B.5}$$

and

$$\alpha_i = \begin{bmatrix} 0 & \sigma_i \\ \sigma_i & 0 \end{bmatrix} \quad \text{and} \quad \beta = \begin{bmatrix} \mathbb{1} & 0 \\ 0 & -\mathbb{1} \end{bmatrix} \tag{B.6}$$

where σ_i are the Pauli matrices

$$\sigma_1 = \begin{bmatrix} 0 & 1 \\ 1 & 0 \end{bmatrix} \quad \text{and} \quad \sigma_2 = \begin{bmatrix} 0 & -i \\ i & 0 \end{bmatrix} \quad \text{and} \quad \sigma_3 = \begin{bmatrix} 1 & 0 \\ 0 & -1 \end{bmatrix}. \tag{B.7}$$

It is possible to decouple the Dirac Hamiltonian through the FW transformation and obtain the non-relativistic limit. We want to semi-decouple the equation. Modifying the H we obtain

$$H = c\boldsymbol{\alpha}\cdot(\boldsymbol{p} + e\boldsymbol{A_0}) + ce\boldsymbol{\alpha}\cdot(\boldsymbol{A} - \boldsymbol{A_0}) + \beta mc^2 + \mathbb{1}V, \tag{B.8}$$

where $\boldsymbol{A_0}$ is the dipole approximated $\boldsymbol{A}$ field. We want to eliminate the second term in eq. (B.8), $ce\boldsymbol{\alpha}\cdot(\boldsymbol{A} - \boldsymbol{A_0})$, and decouple the terms that contains A. Utilize the same method as the FW transformation in [17] we define

$$o = c\boldsymbol{\alpha}\cdot(\boldsymbol{p} + e\boldsymbol{A_0}) \quad \text{and} \quad a = ce\boldsymbol{\alpha}\cdot(\boldsymbol{A} - \boldsymbol{A_0}) \quad \text{and} \quad \varepsilon = \mathbb{1}V, \tag{B.9}$$

and the H then take the form

$$H = o + a + \beta mc^2 + \varepsilon. \tag{B.10}$$

Utilizing the unitary transformation

$$\psi' = e^{+iS}\psi \tag{B.11}$$

the Dirac equation becomes

$$i\frac{\partial\psi'}{\partial t} = \left[e^{+iS}\left(H - i\frac{\partial}{\partial t}\right)e^{-iS}\right]\psi' = H'\psi' \tag{B.12}$$

and the transformed Hamiltonian can be expressed as

$$H' = UHU^\dagger - iU\dot{U}^\dagger = UHU^\dagger - U\dot{S}U^\dagger \tag{B.13}$$

Utilizing the Baker-Campbell Hausdorff formula [2]:

$$e^{ia}be^{-ia} = b + \frac{i}{1!}[a,b] + \frac{i^2}{2!}[a,[a,b]]\ldots, \tag{B.14}$$

the H' becomes

$$H' = H + i[S,H] - \frac{1}{2}[S,[S,H]] - \frac{i}{6}[S,[S,[S,H]]] + \cdots + -\dot{S} - \frac{i}{2}[S,\dot{S}] + \ldots. \tag{B.15}$$

Constructing S by just considering the terms through the order of unity [17],

$$H' = o + a + \varepsilon + \beta mc^2 + i[S,\beta]mc^2. \tag{B.16}$$

Wanting to eliminate the a term , we need to construct S such that $i[S,\beta]mc^2 = -a$, hence,

$$S = -\frac{i\beta a}{2mc^2}. \tag{B.17}$$

The commutations relation in eq.(B.15) then becomes:

$$\begin{aligned} i[S,H] &= i\left[-\frac{i\beta a}{2mc^2}, o + a + \varepsilon + \beta mc^2\right] \\ &= \frac{1}{2mc^2}[\beta a o - o\beta a \\ &+ \quad \beta a a - a\beta a \\ &+ \quad \beta a\varepsilon - \varepsilon\beta a \\ &+ \quad \beta a\beta mc^2 - \beta mc^2\beta a] \\ &= \frac{\beta\{a,o\}}{2mc^2} + \frac{\beta a^2}{mc^2} - a + \frac{\beta}{2mc^2}[a,\varepsilon], \end{aligned} \tag{B.18}$$

$$\begin{aligned} -\frac{1}{2}[S,[S,H]] &= \frac{1}{4mc^2}\left[\beta a, \frac{\beta\{a,o\}}{2mc^2} + \frac{\beta a^2}{mc^2} - a + \frac{\beta}{2mc^2}[a,\varepsilon]\right] \\ &= -\frac{\{a,\{a,o\}\}}{8m^2c^4} - \frac{a^3}{2m^2c^4} - \frac{\beta a^2}{2mc^2} - \frac{1}{8m^2c^4}[a,[a,\varepsilon]], \end{aligned} \tag{B.19}$$

$$\begin{aligned} \frac{i^3}{3!}[S,[S,[S,H]]] &= \frac{1}{6mc^2}\left[\beta a, -\frac{\{a,\{a,o\}\}}{8m^2c^4} - \frac{a^3}{2m^2c^4} - \frac{\beta a^2}{2mc^2} - \frac{1}{8m^2c^4}[a,[a,\varepsilon]]\right] \\ &= -\frac{\{a,\{a,\{a,o\}\}\}}{6\cdot 8m^3c^6} - \frac{\beta a^4}{6m^3c^6} + \frac{a^3}{6m^2c^4}, \end{aligned} \tag{B.20}$$

$$\begin{aligned} \frac{i^4}{4!}[S,[S,[S,[S,H]]]] &= \frac{1}{8mc^2}\left[\beta a, -\frac{\{a,\{a,\{a,o\}\}\}}{6\cdot 8m^3c^6} - \frac{\beta a^4}{6m^3c^6} + \frac{a^3}{6m^2c^4}\right] \\ &= \frac{\beta a^4}{24m^3c^6}, \end{aligned} \tag{B.21}$$

$$\dot{S} = -\frac{i\beta\dot{a}}{2mc^2} \tag{B.22}$$

and

$$\begin{aligned} -\frac{i}{2}[S,\dot{S}] &= \frac{i}{8m^2c^4}[\beta a, \beta\dot{a}] \\ &= -\frac{i}{8m^2c^4}[a,\dot{a}]. \end{aligned} \tag{B.23}$$

The H' then takes the form,

$$\begin{aligned} H' &= o + \varepsilon + \beta mc^2 \\ &+ \beta\frac{\{a,o\}}{2mc^2} + \beta\frac{a^2}{2mc^2} \\ &- \frac{1}{8m^2c^4}[a,[a,\varepsilon]] - \beta\frac{\{a,\{a,\{a,o\}\}\}}{48m^3c^6} - \beta\frac{a^4}{8m^2c^4} - \frac{i}{8m^2c^4}[a,\dot{a}] \\ &+ \beta\frac{1}{2mc^2}[a,\varepsilon] - \frac{\{a,\{a,o\}\}}{8m^2c^4} - \frac{a^3}{3m^2c^4} + \beta\frac{i}{2mc^2}\dot{a}. \end{aligned} \tag{B.24}$$

Separating the even and odd terms and sorting them by order, we define

$$\varepsilon_1' = +\beta\frac{\{a,o\}}{2mc^2} + \beta\frac{a^2}{2mc^2} + \varepsilon, \tag{B.25}$$

$$\varepsilon_2' = -\frac{1}{8m^2c^4}[a,[a,\varepsilon]] - \beta\frac{\{a,\{a,\{a,o\}\}\}}{48m^3c^6} - \beta\frac{a^4}{8m^3c^6} - \frac{i}{8m^2c^4}[a,\dot{a}], \tag{B.26}$$

and

$$a' = \beta\frac{1}{2mc^2}[a,\varepsilon] - \frac{\{a,\{a,o\}\}}{8m^2c^4} - \frac{a^3}{3m^2c^4} + \beta\frac{i}{2mc^2}\dot{a}, \tag{B.27}$$

where ε_1' is of $\mathcal{O}(1)$ and is considered even, ε_2' is of $\mathcal{O}\left(\frac{1}{c^2}\right)$ and is considered even, and a' is of $\mathcal{O}\left(\frac{1}{c}\right)$ and are considered odd. Eliminating the a' term, we choose a new transformation with $S = \frac{-i\beta a'}{2mc^2}$. The only computation relation for this transformation of order $\mathcal{O}\left(\frac{1}{c^2}\right)$ or lower is

$$\begin{aligned} i[S',H'] &= \frac{1}{2mc^2}[\beta a', o + \varepsilon_1' + \varepsilon_2' + a' + \beta mc^2] \\ &= \frac{\beta}{2mc^2}\{a',o\} - a', \end{aligned} \tag{B.28}$$

and H'' becomes,

$$H'' = o + \varepsilon_1' + \varepsilon_2' + \beta mc^2 + \frac{\beta}{2mc^2}\{a',o\}. \tag{B.29}$$

Calculation each of the commutation and anti-commutation relation:

$$\begin{aligned} \{a,o\} &= c^2 e\{\boldsymbol{\alpha}\cdot(\boldsymbol{A}-\boldsymbol{A_0}), \boldsymbol{\alpha}\cdot(\boldsymbol{p}+e\boldsymbol{A_0})\} \\ &= c^2 e(\boldsymbol{\alpha}\cdot(\boldsymbol{A}-\boldsymbol{A_0})\alpha\cdot(\boldsymbol{p}+e\boldsymbol{A_0}) + \boldsymbol{\alpha}\cdot(\boldsymbol{p}+e\boldsymbol{A_0})\boldsymbol{\alpha}\cdot(\boldsymbol{A}-\boldsymbol{A_0})) \\ &= c^2 e(2\boldsymbol{\alpha}^2(\boldsymbol{A}-\boldsymbol{A_0})(\boldsymbol{p}+e\boldsymbol{A_0}) - i\boldsymbol{\alpha}\cdot\nabla(\boldsymbol{\alpha}\cdot(\boldsymbol{A}-\boldsymbol{A_0})) \\ &= c^2 e(2(\boldsymbol{A}-\boldsymbol{A_0})\cdot(\boldsymbol{p}+e\boldsymbol{A_0}) + \boldsymbol{\sigma}_{4\times4}\cdot\nabla\times(\boldsymbol{A}-\boldsymbol{A_0})) \\ &= c^2 e(2(\boldsymbol{A}-\boldsymbol{A_0})\cdot(\boldsymbol{p}+e\boldsymbol{A_0}) + \boldsymbol{\sigma}_{4\times4}\cdot\boldsymbol{B}), \end{aligned} \tag{B.30}$$

where the matrix $\boldsymbol{\sigma_{4\times4}}$ is defined as,

$$\boldsymbol{\sigma}_{4\times4} = \begin{bmatrix} \boldsymbol{\sigma} & 0 \\ 0 & \boldsymbol{\sigma} \end{bmatrix}. \tag{B.31}$$

The $\boldsymbol{\sigma}_{4\times4}$ is even and therefore does not couple the large and small components. Here we used the fact the $\boldsymbol{\alpha}$ is constructed utilizing Pauli matrices and they follow this relation [17],

$$\boldsymbol{\sigma}\cdot\boldsymbol{a}\,\boldsymbol{\sigma}\cdot\boldsymbol{b} = \boldsymbol{a}\cdot\boldsymbol{b} + i\boldsymbol{\sigma}\cdot\boldsymbol{a}\times\boldsymbol{b}. \tag{B.32}$$

$$\begin{aligned}\{a,\{a,o\}\} =& c^3e^2\{\boldsymbol{\alpha}\cdot(\boldsymbol{A}-\boldsymbol{A_0}),2(\boldsymbol{A}-\boldsymbol{A_0})\cdot(\boldsymbol{p}+e\boldsymbol{A_0})+\boldsymbol{\sigma}_{4\times4}\cdot\boldsymbol{B}\}\\ =& c^3e^2(4\boldsymbol{\alpha}\cdot(\boldsymbol{A}-\boldsymbol{A_0})(\boldsymbol{A}-\boldsymbol{A_0})\cdot(\boldsymbol{p}+e\boldsymbol{A_0})+2\boldsymbol{\sigma}_{4\times4}\cdot\boldsymbol{B}\boldsymbol{\alpha}\cdot(\boldsymbol{A}-\boldsymbol{A_0}))\end{aligned} \tag{B.33}$$

$$\{a,\{a,\{a,o\}\}\} = 4c^4e^3\left(2(\boldsymbol{A}-\boldsymbol{A_0})^3\cdot(\boldsymbol{p}+e\boldsymbol{A_0})+(\boldsymbol{A}-\boldsymbol{A_0})^2\boldsymbol{\sigma}_{4\times4}\cdot\boldsymbol{B}\right) \tag{B.34}$$

The more trivial terms:

$$a^2 = c^2e^2(\boldsymbol{A}-\boldsymbol{A_0})^2 \tag{B.35}$$

$$a^3 = c^3e^3\boldsymbol{\alpha}\cdot(\boldsymbol{A}-\boldsymbol{A_0})^3 \tag{B.36}$$

$$a^4 = c^4e^4(\boldsymbol{A}-\boldsymbol{A_0})^4 \tag{B.37}$$

$$\dot{a} = ce\boldsymbol{\alpha}\cdot(\dot{\boldsymbol{A}}-\dot{\boldsymbol{A}}_{\boldsymbol{0}}) \tag{B.38}$$

$$[a,\varepsilon]=0 \Rightarrow [a,[a,\varepsilon]]=0 \tag{B.39}$$

$$[a,\dot{a}]=0 \tag{B.40}$$

Next, we can construct the correction terms, ε_1' and ε_2',

$$\varepsilon_1' = V+\beta\left(\frac{e^2\boldsymbol{A}^2}{2m}-\frac{e^2\boldsymbol{A_0}^2}{2m}+\frac{e(\boldsymbol{A}-\boldsymbol{A_0})\cdot\boldsymbol{p}}{m}+\frac{e\boldsymbol{\sigma}_{4\times4}\cdot\boldsymbol{B}}{2m}\right), \tag{B.41}$$

and

$$\begin{aligned}\varepsilon_2' =& -\beta\frac{e^3}{6m^3c^2}(\boldsymbol{A}-\boldsymbol{A_0})^3\cdot(\boldsymbol{p}+e\boldsymbol{A_0})-\beta\frac{e^4}{8m^3c^2}(\boldsymbol{A}-\boldsymbol{A_0})^4\\ &-\beta\frac{e^3}{12m^3c^2}(\boldsymbol{A}-\boldsymbol{A_0})^2\boldsymbol{\sigma}_{4\times4}\cdot\boldsymbol{B}.\end{aligned} \tag{B.42}$$

Now the $\{a',o\}$ anti commutation,

$$\{a',o\} = -\frac{\{\{a,\{a,o\}\},o\}}{8m^2c^4}-\frac{\{a^3,o\}}{3m^2c^4}+\frac{\{i\beta\dot{a},o\}}{2mc^2} \tag{B.43}$$

and the corresponding correction terms become

$$\frac{\beta}{2mc^2}\{a',o\} = -\frac{\beta}{2mc^2}\frac{\{\{a,\{a,o\}\},o\}}{8m^2c^4}-\frac{\beta}{2mc^2}\frac{\{a^3,o\}}{3m^2c^4}+\frac{\beta}{2mc^2}\frac{\{i\beta\dot{a},o\}}{2mc^2}. \tag{B.44}$$

Starting with $\{i\beta\dot{a},o\}$ term,

$$\frac{\beta}{2mc^2}\frac{\{i\beta\dot{a},o\}}{2mc^2} = \frac{e\boldsymbol{\sigma}_{4\times4}\cdot((\boldsymbol{E}-\boldsymbol{E_0})\times(\boldsymbol{p}+e\boldsymbol{A_0})}{2m^2c^2}+\frac{e\nabla\cdot(\boldsymbol{E}-\boldsymbol{E_0})}{4m^2c^2}+\frac{ie\boldsymbol{\sigma}_{4\times4}\cdot\nabla\times(\boldsymbol{E}-\boldsymbol{E_0})}{4m^2c^2}, \tag{B.45}$$

where

$$\dot{\boldsymbol{A}}-\dot{\boldsymbol{A}}_{\boldsymbol{0}} = -(\boldsymbol{E}-\boldsymbol{E_0}). \tag{B.46}$$

The $\{a^3,o\}$ term becomes

$$-\frac{\beta}{2mc^2}\frac{\{a^3,o\}}{3m^2c^4} = \beta\left(-\frac{e^3}{3m^3c^2}(\boldsymbol{A}-\boldsymbol{A_0})^3(\boldsymbol{p}+e\boldsymbol{A_0})-\frac{e^3}{6m^3c^2}(\boldsymbol{A}-\boldsymbol{A_0})^2\boldsymbol{\sigma}_{4\times4}\cdot\boldsymbol{B}\right), \tag{B.47}$$

and the $\{\{a,\{a,o\}\},o\}$ term can be expressed as

$$\begin{aligned}-\frac{\beta}{2mc^2}\frac{\{\{a,\{a,o\}\},o\}}{8m^2c^4} =& -\frac{\beta}{2m^3c^2}(\boldsymbol{A}-\boldsymbol{A_0})\cdot(\boldsymbol{p}+e\boldsymbol{A_0})(\boldsymbol{A}-\boldsymbol{A_0})\cdot(\boldsymbol{p}+e\boldsymbol{A_0})\\ &-\beta\frac{e^2}{2m^3c^2}\boldsymbol{\sigma}_{4\times4}\cdot\boldsymbol{B}(\boldsymbol{A}-\boldsymbol{A_0})\cdot(\boldsymbol{p}+e\boldsymbol{A_0})-\beta\frac{e^2}{8m^3c^2}\boldsymbol{B}^2.\end{aligned} \tag{B.48}$$

Combining these, the $\{a',o\}$ correction term becomes

$$\begin{aligned}\frac{\beta}{2mc^2}\{a',o\} =& -\beta\frac{e^2}{2m^3c^2}(\boldsymbol{A}-\boldsymbol{A_0})\cdot(\boldsymbol{p}+e\boldsymbol{A_0})(\boldsymbol{A}-\boldsymbol{A_0})\cdot(\boldsymbol{p}+e\boldsymbol{A_0})\\ &-\beta\frac{e^2}{2m^3c^2}\boldsymbol{\sigma}_{4\times4}\cdot\boldsymbol{B}(\boldsymbol{A}-\boldsymbol{A_0})\cdot(\boldsymbol{p}+e\boldsymbol{A_0})-\frac{\beta e^2}{8m^3c^2}\boldsymbol{B}^2\\ &-\beta\frac{e^3}{3m^3c^2}(\boldsymbol{A}-\boldsymbol{A_0})^3(\boldsymbol{p}+e\boldsymbol{A_0})-\beta\frac{e^3}{6m^3c^2}(\boldsymbol{A}-\boldsymbol{A_0})^2\boldsymbol{\sigma}_{4\times4}\cdot\boldsymbol{B}\\ &+\frac{e\boldsymbol{\sigma}_{4\times4}\cdot(\boldsymbol{E}\times(\boldsymbol{p}+e\boldsymbol{A_0})}{2m^2c^2}+\frac{e\nabla\cdot\boldsymbol{E}}{4m^2c^2}+\frac{ie\boldsymbol{\sigma}_{4\times4}\cdot\nabla\times\boldsymbol{E}}{4m^2c^2}\end{aligned} \tag{B.49}$$

The compressed new Hamiltonian is expressed as

$$\begin{aligned}H'' =& c\boldsymbol{\alpha}\cdot(\boldsymbol{p}+e\boldsymbol{A_0})+\beta mc^2+\mathbb{1}V\\ &+\beta\left(\frac{e^2\boldsymbol{A}^2}{2m}-\frac{e^2{\boldsymbol{A_0}}^2}{2m}+\frac{e(\boldsymbol{A}-\boldsymbol{A_0})\cdot\boldsymbol{p}}{m}+\frac{e\boldsymbol{\sigma}_{4\times4}\cdot\boldsymbol{B}}{2m}\right)\\ &-\beta\frac{e^4}{8m^3c^2}(\boldsymbol{A}^2-{\boldsymbol{A_0}}^2)^2-\beta\frac{e^3}{2m^3c^2}(\boldsymbol{A}^2-{\boldsymbol{A_0}}^2)(\boldsymbol{A}-\boldsymbol{A_0})\cdot\boldsymbol{p}\\ &-\beta\frac{e^2}{2m^3c^2}(\boldsymbol{A}-\boldsymbol{A_0})\cdot\boldsymbol{p}(\boldsymbol{A}-\boldsymbol{A_0})\cdot\boldsymbol{p}-\beta\frac{e^2}{8m^3c^2}\boldsymbol{B}^2\\ &-\beta\frac{e^3}{4m^3c^2}(\boldsymbol{A}-\boldsymbol{A_0})^2\boldsymbol{\sigma}_{4\times4}\cdot\boldsymbol{B}-\beta\frac{e^2}{2m^3c^2}\boldsymbol{\sigma}_{4\times4}\cdot\boldsymbol{B}(\boldsymbol{A}-\boldsymbol{A_0})\cdot(\boldsymbol{p}+e\boldsymbol{A_0})\\ &+\frac{e\boldsymbol{\sigma}_{4\times4}\cdot((\boldsymbol{E}-\boldsymbol{E_0})\times(\boldsymbol{p}+e\boldsymbol{A_0})}{2m^2c^2}+\frac{e\nabla\cdot(\boldsymbol{E}-\boldsymbol{E_0})}{4m^2c^2}-\frac{ie\boldsymbol{\sigma}_{4\times4}\cdot\dot{\boldsymbol{B}}}{4m^2c^2}.\end{aligned} \tag{B.50}$$

This Hamiltonian consists of the dipole approximated Dirac Hamiltonian, with beyond dipole correction terms. The Hamiltonian conserves many of the relativistic structural effects in dipole terms, and we have the $\boldsymbol{A}^2(x,t)$ explicitly in the Hamiltonian. Another advantage is that by Taylor expanding the vector potential, the order of many of the correction terms becomes greater than $\mathcal{O}\left(\frac{1}{c^2}\right)$ and we are left with,

$$\begin{aligned}H'' =& c\boldsymbol{\alpha}\cdot(\boldsymbol{p}+e\boldsymbol{A_0})+\beta mc^2+\mathbb{1}V\\ &+\beta\left(\frac{e^2\boldsymbol{A}^2}{2m}-\frac{e^2{\boldsymbol{A_0}}^2}{2m}+\frac{e(\boldsymbol{A}-\boldsymbol{A_0})\cdot\boldsymbol{p}}{m}+\frac{e\boldsymbol{\sigma}_{4\times4}\cdot\boldsymbol{B}}{2m}\right)+\mathcal{O}\left(\frac{1}{c^3}\right).\end{aligned} \tag{B.51}$$

This Hamiltonian is being implemented and tested by the research group and is giving promising results [34].

Bibliography

[1] Morten Førre. Breakdown of the nonrelativistic approximation in superintense laser-matter interactions. *PHYSICAL REVIEW A*, 99(053410), March 2019.

[2] Morten Førre and Sølve Selstø. Schrödinger formulation of the nondipole light-matter interaction consistent with relativity. *Phys. Rev. A*, 101:063416, Jun 2020.

[3] M. Planck. On the theory of the energy distribution law of the normal spectrum. *Verhandl. Dtsch. phys. Ges.*, 2, 1900.

[4] Ronald Friedman Peter Atkins. *Molecular Quantum Mechanics*. Oxford University Press Inc., New York, 5 edition, 2011.

[5] E. Schrödinger. An undulatory theory of the mechanics of atoms and molecules. *Phys. Rev.*, 28:1049–1070, Dec 1926.

[6] W. Heisenberg. Über den anschaulichen inhalt der quantentheoretischen kinematik und mechanik. z. *Physik*, 43:172–198, March 1927.

[7] P. A. M. Dirac. The quantum theory of the electron. *Proceedings of the Royal Society of London. Series A, Containing Papers of a Mathematical and Physical Character*, 117(778):610–624, 1928.

[8] N. Bohr Dr. phil. I. on the constitution of atoms and molecules. *The London, Edinburgh, and Dublin Philosophical Magazine and Journal of Science*, 26(151):1–25, 1913.

[9] A. Einstein. Über einen die erzeugung und verwandlung des lichtes betreffenden heuristischen gesichtspunkt. *Annalen der Physik*, 322(6):132–148, 1905.

[10] A. Einstein. Über die von der molekularkinetischen theorie der wärme geforderte bewegung von in ruhenden flüssigkeiten suspendierten teilchen. *Annalen der Physik*, 322(8):549–560, 1905.

[11] A. Einstein. Zur elektrodynamik bewegter körper. *Annalen der Physik*, 322(10):891–921, 1905.

[12] A. Einstein. Ist die trägheit eines körpers von seinem energieinhalt abhängig? *Annalen der Physik*, 323(13):639–641, 1905.

[13] Jeff Hecht. Short history of laser development. *Applied optics*, 49:F99–122, 09 2010.

[14] Albert Einstein. *The Collected Papers of Albert Einstein, Volume 6 (English): The Berlin Years: Writings, 1914-1917. (English translation supplement)*, volume 6. Princeton University Press, 1997.

[15] V. Yanovsky, V. Chvykov, G. Kalinchenko, P. Rousseau, T. Planchon, T. Matsuoka, A. Maksimchuk, J. Nees, G. Cheriaux, G. Mourou, and K. Krushelnick. Ultra-high intensity- 300-tw laser at 0.1 hz repetition rate. *Opt. Express*, 16(3):2109–2114, Feb 2008.

[16] A. Ansón-Casaos, J. C. Ciria, O. Sanahuja-Parejo, S. Víctor-Román, J. M. González-Domínguez, E. García-Bordejé, A. M. Benito, and W. K. Maser. The viscosity of dilute carbon nanotube (1d) and graphene oxide (2d) nanofluids. *Phys. Chem. Chem. Phys.*, 22:11474–11484, 2020.

[17] S. D. Drell J. D. Bjorken. *Relativistic Quantum Mechanics:International series in pure and applied physics*. McGraw-Hill, Inc., Stanford University, 1964.

[18] R. A. Freedman H. D. Young. *University Physics with modern physics*. Pearson, University of California, 14 edition, 2014.

[19] A. Poszwa J. Karwowski1, A. Ishkanyan. The eigenvalue problem of one-dimensional dirac operator. *Theoretical Chemistry Accounts*, 139(178), November 2020.

[20] Walter Greiner. *Relativistic Quantum Mechanics*. Springer, Berlin, Heidelberg, 3 edition, 2000.

[21] David J. Griffits and Reed College. *Introduction to electrodynamics*. Prentice Hall, Upper Saddle River, New Jersey, 3 edition, 1999.

[22] J. A. Heras. How the potentials in different gauges yield the same retarded electric and magnetic fields. *Am. J. Phys.*, 75(176), January 2007.

[23] Kharanshu Solanki. An overview of semi-classical light-matter interactions, 06 2022.

[24] S. Weinberg. *Molecular Quantum Mechanics*, volume 1 Foundations. Cambridge University Press, University of Texas Austin, 2005.

[25] Morten Førre and Aleksander Skjerlie Simonsen. Nondipole ionization dynamics in atoms induced by intense xuv laser fields. *Phys. Rev. A*, 90:053411, Nov 2014.

[26] Hadi Tokmehdashi, Ali Akbar Rajabi, and Majid Hamzavi. Dirac equation with mixed scalarvectorpseudoscalar linear potential under relativistic symmetries. *Zeitschrift für Naturforschung A*, 70(9):713–720, 2015.

[27] P. Alberto, Carlos Fiolhais, and V Gil. Relativistic particle in a box. *European Journal of Physics*, 17:19, 01 1996.

[28] V. A. Yerokin V. M. Shabaev, I. I. Tupitsyn, G. Plunien, and G.Soff. Dual kinentic balance approach to basis-set expansions for dirac equation. *Physical Review Letter*, 93(13), September 2004.

[29] S. W. Hawking and Thomas Hertog. Living with ghosts. *Phys. Rev. D*, 65:103515, May 2002.

[30] Michael Edward Peskin and Daniel V. Schroeder. *An Introduction to Quantum Field Theory*. Westview Press, 1995. Reading, USA: Addison-Wesley (1995) 842 p.

[31] M. Alamgir Hossain and Mostak Ahmed. Application of gauss legendre quadrature rule for solving initial value problems. 11 2011.

[32] Greg Von Winckel. lglnodes.m. Matlab, April 2004.

[33] Andreas Oskar Herland Dalseng. *Identifying relativistic effects in the light-matter interaction between a high-intensity laser pulse and a one-dimensional atomic model.* PhD thesis, University of Bergen, 2021.

[34] Morten Førre. Private comununication. 2022.

[35] A. S. Simonsen. *Two-Photon Double Ionisation of H_2.* PhD thesis, University of Bergen, 2012.

[36] J. Liu and Y. Hao. Cranknicolson method for solving uncertain heat equation. *Soft Comput*, 26:937–945, January 2022.

[37] Youcef Saad and Martin H. Schultz. Gmres: A generalized minimal residual algorithm for solving nonsymmetric linear systems. *SIAM Journal on Scientific and Statistical Computing*, 7(3):856–869, 1986.

[38] Brian Moore. lanczosprop.m. Matlab, July 2013.

[39] A. S. Simonsen. *Simulation of Atoms in superintens Laser Fields by solving the time dependent Schordinger equation.* PhD thesis, University of Bergen, April 2016.

[40] Y. Saad. *Iterative Methods for Sphars Linear System.* Society for Industrial and applied Matmatics, 2003.

[41] Tor Kjellsson, Sølve Selstø, and Eva Lindroth. Relativistic ionization dynamics for a hydrogen atom exposed to superintense xuv laser pulses. *Phys. Rev. A*, 95:043403, Apr 2017.